JPRS-JST-90-054
4 DECEMBER 1990

FOREIGN BROADCAST INFORMATION SERVICE

JPRS Report

Science & Technology

Japan

STRUCTURE, PROPERTIES OF AL AMORPHOUS ALLOYS

JPRS-JST-90-054
4 DECEMBER 1990

SCIENCE & TECHNOLOGY
JAPAN

STRUCTURE, PROPERTIES OF AL AMORPHOUS ALLOYS

906C7531 Tokyo AL KEI AMORUFASU GOKIN NO KOZO TO TOKUSEI in Japanese 6 Feb 90 pp 1-40

[Papers presented at the Symposium for Structure and Properties of Al Amorphous Alloys, held 6 Feb 90 in Tokyo and sponsored by the Japan Institute of Metals]

CONTENTS

Thermodynamics for Formation of Amorphous Materials

906C7531A Tokyo AL KEI AMORUFASU GOKIN NO KOZO TO TOKUSEI in Japanese 6 Feb 90 pp 1-4

[Article by Keiichi Ishihara, Department of Technology, Kyoto University]

[Text] **1. What Is Thermodynamics?**

Where the phase change, that is, a chemical reaction A→B is concerned, and providing both the reactant A and the product B undergo no changes in their chemical potentials, we learn from thermodynamics the direction in which the reaction proceeds spontaneously at a constant pressure (or a constant volume) and a constant temperature, that is, the reaction proceeds to the side where the Gibbs free energy is lower (in the case of constant temperature and pressure).

Although thermodynamics affords us the direction of spontaneous change, it is not concerned with the question of whether the reaction actually takes place or not. For example, with diamond being less stable than graphite and its free energy smaller than the latter at a constant temperature and pressure, one may reasonably suppose that it turns spontaneously into graphite. Nevertheless, it will continue to be as it is in the stable state and be used as a jewel and a grinding material. It is absolutely certain, on the other hand, that graphite is not converted to diamond at a constant temperature and pressure. Briefly, we learn from thermodynamics only whether the occurrence of a reaction is possible or not.

In connection with the discussion on the formation of amorphous materials in terms of thermodynamics to follow, it is to be pointed out that the reactions in question do not necessarily occur in all cases, but that the discussion is concerned only with the possibility of the occurrence of the reaction. Although one may suspect the usefulness of thermodynamics from the above, it is much better to know only the possibility of the occurrence of a reaction than to know nothing about the reaction.

2. Amorphous State Free Energy

Where the formation of an amorphous material is concerned, it is important to estimate the free energy of the amorphous material produced. The amorphous state, a solid state exhibiting a short-range regularity but lacking a long-range one in terms of structure, is not amenable to definition in terms of thermodynamics. The amorphous state, in general, is taken as the one in which a supercooled liquid is frozen into, and the relevant change is referred to as the glass transition, which might be taken as a phase transition of the second order and which rarely falls into the category of purely thermodynamic phase transition because the relevant temperature, the glass transition temperature, T_g, varies with the cooling rate, among other things.

The free energy of the alloy $Te_{85}Ge_{15}$ in the amorphous state, as estimated empirically by measurement of its specific heat at temperatures below its glass transition point, etc., has proved to be some 300 J/mol larger than that for the supercooled liquid at a temperature 100 K below its T_g.[1,2] However, the relevant values for the general series of alloys available are almost nil. Practically, as it is dealt with here, the free energy of a material in the amorphous state may be taken to be approximately equal to that of the supercooled liquid.

3. Formation of Amorphous State Materials by Different Processes

Of the methods of manufacture of amorphous metals—metals alone are dealt with here—that of rapid solidification are generally known. Others included are: vapor deposition, sputtering, and other vapor-phase synthesis (plasma included); ionic radiation; and mechanical alloying, the one that has been recently in the limelight.[3] Formation of materials in the amorphous state is discussed thermodynamically for each process in this section.[3]

(1) Rapid Solidification

With the reader being referred to many relevant introductory writings available,[4,5] the subject is briefly dealt with here. This method involves heating of an alloy above its melting point to turn the alloy into the complete liquid state and, subsequently, cooling it rapidly. The rate of cooling must be 10^6K/s, or more if an amorphous alloy is to be afforded. The free energy of the reactant, being a liquid, would desirably be compared here with that of the alloy in the amorphous state; nevertheless, thermodynamics is not available under such a condition of rapid temperature change. The method is, however, just in line with the definition of the amorphous state given in the preceding section, and any alloy must be turned into the amorphous state if the rate of cooling is sufficiently rapid. The question of the amorphous state thus seems to be entirely in the category of the kinetic theory and to have nothing to do with the thermodynamics. However, there exist restricting conditions for the presence of the supercooled state and the amorphous state, such as the following:

1) The supercooled liquid needs to be stable as liquid (whether compared with relevant solid states or not).

2) It needs to be reluctant to turn into a stable solid phase.

Thermodynamics is very useful at this juncture, that is, we need to examine cases where it is impossible for the supercooled liquid to turn into other phases. As known empirically, metal is reluctant to turn into the amorphous state. Below the temperature T_0 at which the free energy of a supercooled liquid is equal to that of its solid solution, the former is turned readily into the solid solution (because here the liquid is allowed to solidify without diffusion and has itself grown unstable) (Figure 1). Conceivably, those alloy-series or alloy-compositions with a T_g higher than T_0 are more easily turned into the amorphous state.[6] Some alloys, which have their liquid phase decomposed into two phases, in turn, are reluctant to yield the amorphous type. All in all, it may be concluded that an alloy in which a liquid phase is more stable than its solid phase, namely, one with a ΔH (enthalpy of mixing of liquid) negative in sign and larger in magnitude, is more easily formed in the amorphous state.

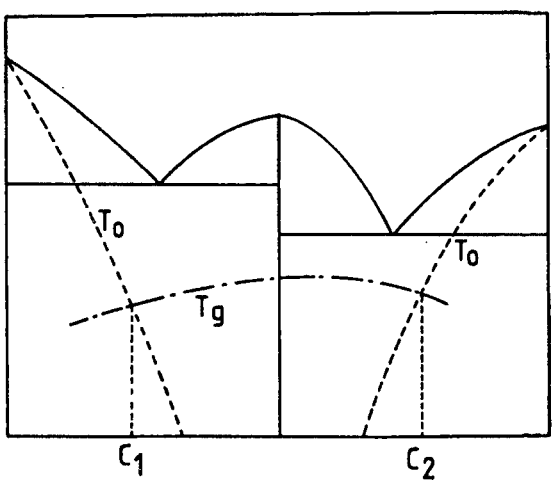

Figure 1. Imaginary- or Model-Constitutional Diagram (Indicating that formation of an amorphous alloy is possible in the composition range from C_1 to C_2.)

(2) Mechanical Alloying

In mechanical alloying, pure metals are allowed to react by means of mechanical mixing. The rise of temperature is almost nil in this case, with the reaction conceivably taking place at low temperature; the reaction is amenable to thermodynamic analysis, namely, materials may be turned into the amorphous state in the case of a series of materials or compositions wherein the free energy of the mixture of pure metals, the reactants, is greater than that of the relevant supercooled liquid. Where the report that an amorphous material was turned out from intermetallic compounds that have the lowest free energy—a phenomenon in contradiction to a thermodynamic rule, since an increase in free energy is involved in this process—one needs simply to note that a mechanical energy had been added in the process and hence an increase in free energy. How much mechanical energy is necessary to change the free energy of the solid system?

In the first place, where changes in microstructure are concerned, the alloy Ag-Fe, which scarcely allows conversion from the liquid phase to solid solution, for example, affords a fine microstructure of the order of several tens of nm when subjected to mechanical alloying. The free energy of this fine structure may conceivably have risen by the amount of the interfacial energy added. Figure 2 presents the enthalpy built up in the course of mechanical alloying for the alloy series Ag-Cu, as estimated by differential scan calorimetry (DSC) along with those for each phase.[7]

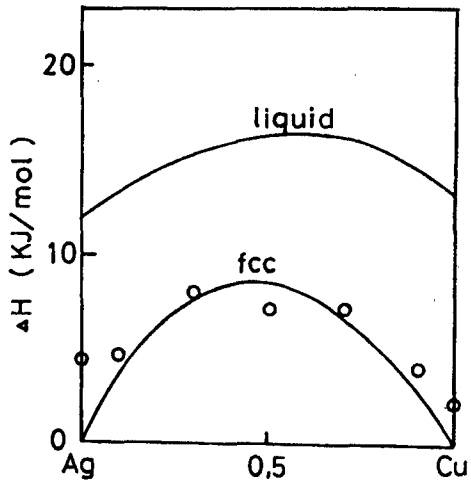

Figure 2. Energy Buildup (denoted by o) and Enthalpies of the Liquid and the Solid Solution for a Mixture of the Powders of Ag and Cu Having Been Subjected to 400 Hours of Mechanical Alloying

The enthalpy so built up is estimated at around 20~40 percent in amount of that of the liquid and may conceivably consist of the one between the same phases and the one between different phases, with the former being proportional to the enthalpy of melting and the latter to that of mixing. It is to be added here that, where the enthalpy of mixing for a liquid is negative, the interfacial energy is also negative, leading to a loss of the energy of the liquid rather than to a buildup. If the mixing is pushed ahead up to the atomic level at all, the energy of the alloy will approach the free energy of the liquid state.[8] In other words, mechanical alloying and mechanical grinding essentially represent a process of creating liquid (supercooled liquid) or the amorphous state. The final product of this process is a supercooled liquid just as it is with rapid solidification, and the series of compositions of alloys involved in the former process are identical with the ones for the latter. The former, nevertheless, is favored in the ease with which to keep the amorphous state produced because of its lower processing temperature.

(3) Other Means

In addition to the above reactions in liquid and solid phases, vapor phase reactions are also available for the relevant purpose. With the vapor phase being at a higher energy level than the liquid and solid phases, the vapor phase reaction may conceivably be more favored than the others in bringing out the amorphous state, and it is needless to say that the supercooled liquid is

more stable in this case than in the others. Briefly, the amorphous state is produced by quench from vapor phases, liquid phases, very fine crystalline phases, etc., at higher energy levels, and the ease with which it is produced depends on the stability of the supercooled liquid.

4. Capacity of Alloys for Forming the Amorphous State

That the enthalpy of mixing to be negative in sign and large in magnitude is a precondition for the formation of amorphous alloys was referred to above, that is, one can predict the question of amorphous state if he has its enthalpy of mixing available for that purpose and, hence, if he has charts of the T_0 curve and of the composition-vs.-free-energy curve as shown in Figures 1 and 2, respectively, available for it. It is evidently necessary to obtain the free energy of alloys as a function of their compositions to work out these charts. Research has been pushed on, in turn, to draw up by calculation a phase diagram on the basis of free energy functions, with free energy functions having been worked out for nearly all two-element alloys.[9] Also available as a systematic study is an empirical formula for computing the enthalpy of mixing, produced by Miedema[10]; one case involving this empirical formula for a ΔH (enthalpy of mixing for 50 percent alloys) of the two element alloy Al-transition metal is shown in Figure 3. It can be seen from the figure that the enthalpy of mixing is negative for almost any transition metal and hence easy formation of relevant amorphous alloys, but that Cu, Mo, Ag, etc., are exceptionally unfavorable as an element of amorphous alloys.

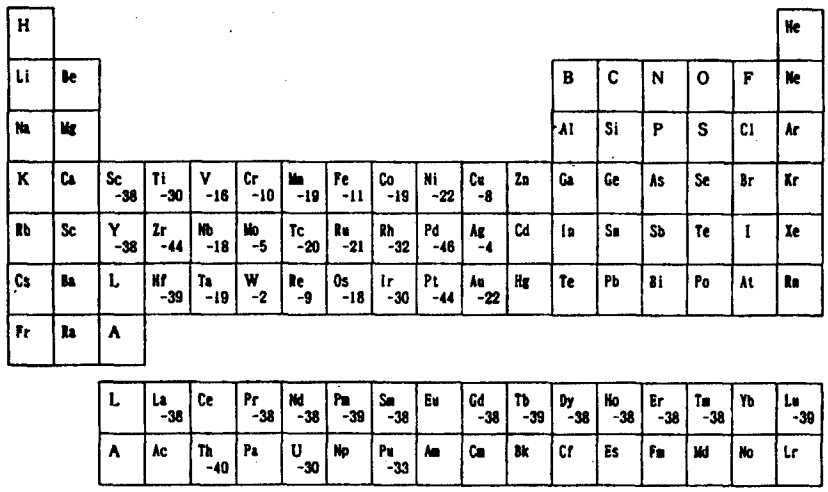

Figure 3. Enthalpies of Mixing for Liquid Phase of Two-Element Alloys Al-Transition Element (in kJ/mol) Computed by Use of Miedema's Formula

References

1. Shinmiya, H., Suzuki, R., and Ishihara, K., SOLID PHYSICS, Vol 20, 1985, p 593.

2. Suzuki, R., "The Thesis for the Masters Degree at the Technology Department of Kyoto University 1985."

3. "A Collection of Feature Articles: Recent Tendency of Research on Mechanical Alloying," JOURNAL OF JAPAN METALLURGY SOCIETY, Vol 27, 1988, p 799.

4. Shinmiya, H. and Ishihara, K., IRON AND STEEL, Vol 69, 1983, p 1087.

5. Shinmiya, H., Suzuki, R., and Ishihara, K., MATERIALS, Vol 33, 1984, p 239.

6. Ishihara, K.N. and Shingu, P.H., MATER. SCI. ENG., Vol 63, 1984, p 251.

7. Murray, J.L., METAL. TRANS., Vol 15A, 1984, p 261.

8. Ishihara, K., Wu, F., Uenishi, K., Hisayama, J., and Shinmiya, H., Summary of lectures for the symposium of the 1989 Fall Convention of the Japan Metallurgy Society, 1989, p 189.

9. The following may prove useful as reference articles:
CALPHAD, Vol 10, 1986, p 255.
BULLETIN OF ALLOY PHASE DIAGRAM, Vol 9, 1988, p 727.

10. Niessen, A.K., de Boer, F.R., Boom, R., de Châtel, R.F., Mattens, W.C.M., and Miedema, A.R., CALPHAD, Vol 7, 1983, p 51.

Glass Transition, Capacity for Amorphous State Formation for Al-Based Amorphous Alloys

906C7531B Tokyo AL KEI AMORUFASU GOKIN NO KOZO TO TOKUSEI in Japanese 6 Feb 90 pp 5-8

[Article by Akihisa Inoue, Research Institute for Iron, Steel, and Other Metals, Tohoku University]

[Text] **1. Introduction**

Amorphous alloys of the Al series are attracting ardent attention because of the prospect of their application as a new type of high-strength material. This is ascribed to the alloys of this series being as important industrially as those of the Fe, Co, Ni, and Ti series, and development of a material in a viscous amorphous phase from this series of alloys, hence, has long been awaited and, further, they characteristically exhibit high specific strength, high corrosion resistance, and a distinct glass transition. This paper deals with the Al-based amorphous alloy series in which glass transition is demonstrable, the relevant composition range,[1] and the effect of the constituting elements of the alloy on the glass transition behavior and on the capacity of amorphous material formation of the alloy.[2]

2. Relationship Between the Appearance of Glass Transition and the Capacity for Turning Into Glass

If an alloy subjected to rapid cooling is to turn amorphous, it is necessary to cool the supercooled liquid down to the glass transition temperature, T_g, while the development and growth of crystal nuclei in temperatures between the melting point T_m and T_g is being blocked. The conditions allowing an alloy to be capable of being readily turned amorphous, therefore, may be cited as a small difference between T_m and T_g of the alloy and the reluctance of the alloy supercooled in the temperature range between T_m and T_g to allow development and growth of its crystal nuclei. It is known that Pt- and Pd-based alloys in the amorphous state, upon heating continuously and raising the temperature at a rate of 2~40 K per minute, turn into the supercooled state before becoming crystallized. The appearance of a region of the supercooled state upon continuous heating of these alloys before the alloys reach the crystallization temperature T_x is understood to be a result of the high stability of the alloys

against crystallization; namely, where alloys like the above showing glass transition at a temperature below T_x are concerned, the liquid supercooled to a temperature below T_m by rapid liquid cooling is highly stable against crystal deposition, can maintain the supercooled state even at comparatively slow cooling rates down to T_g, and hence may conceivably possess a high capacity for glass formation. It is generally conceivable that an alloy has a greater capacity for glass formation because it has a greater region for its supercooled region.

3. Conventional Alloy Series Showing Glass Transition and Relevant Capacities for Forming Amorphous Alloys

To prove the rationale of the above concept, correlation between the temperature difference, ΔT, between T_g and T_x and the critical cooling rate R_c was investigated and is presented in Figure 1 with respect to amorphous alloys for which glass transition has been demonstrated to date. R_c is minimal for those alloys with ΔT above about 50 K, such as Pt and Pd, grows for those with ΔT below 50 K, in the order Pd–Cu–Si, Pd–Si, Fe–P–C series, and rises as high as 10^5K/s for those exhibiting no glass transition. It may thus be concluded that the stability of a supercooled liquid as represented by ΔT_x is highly correlated to the capacity for glass formation of alloys.

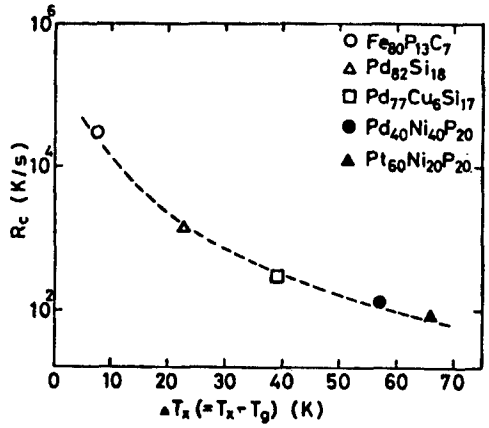

Figure 1. Relationship Between Critical Cooling Rate R_c and ΔT_x (= T_x – T_g) in Amorphous Alloy Formation

4. Al-Based Alloy Series Involving T_g and Range of Relevant Compositions

Figure 2 presents the ranges of compositions for formation of amorphous phases and glass transitions for rapidly cooled three-element alloys Al–Ni–Ln, where Ln denotes Y, La, or Ce. The range for the formation of the amorphous phase is fairly wide, over 0~30 at% for Ni and 2~25 percent for Ln, whereas the one for glass transition is limited and narrow, over 2~11 percent for Ni and 9~11 percent for Y in the case of Al–Ni–Y series and over 7~13 percent for Ni and 5~9 percent for Ln in the cases of Al–Ni–La and Al–Ni–Ce. As can be seen from Figure 3, the compositions allowing T_g to show up is limited to those wherein the process of conversion of amorphous alloy into crystals is shifting from Am→fcc Al + Am′→Al + compound to Am→Al + compound or Am→compound and those

wherein the solute concentrations are slightly higher than the preceding case of compositions. T_g, therefore, is present in the region of composition wherein Al atoms are almost totally combined with the solute atoms Ln and Ni, which behave negatively, and is gone in those wherein the Al content is larger than the former case with the bonding Al–Al present in larger amounts and in those wherein the Ln and Ni contents are larger and the bondings Ln–Ni, Ln–Ln, and Ni–Ni are present in greater amounts.

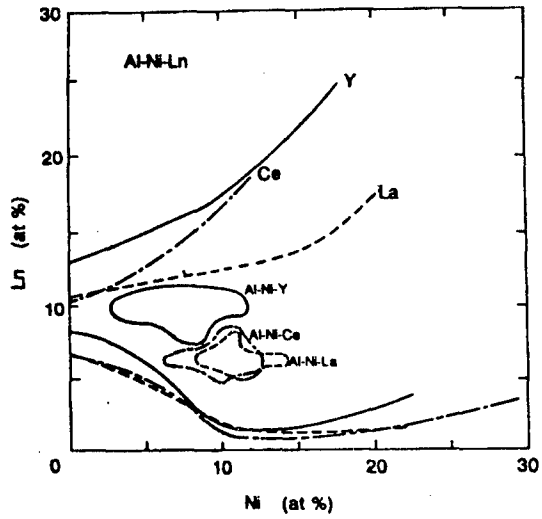

Figure 2. Ranges of Composition for Formation of Amorphous Alloy and for Glass Transition in Three-Element Amorphous Alloy Series Al–Ni–Ln (Ln = Y, La, Ce)

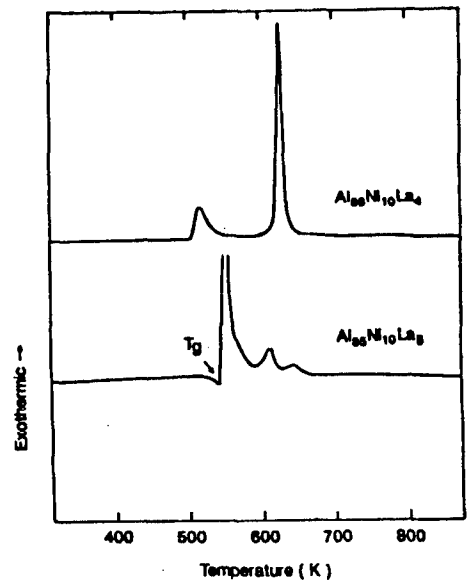

Figure 3. Changes, With Amount of La, of Differential Scanning Calorimetry (DSC) Curve for Amorphous Alloy Series Al–Ni–La

Other Al-based amorphous alloys in which T_g can be seen are those of the Al–Co–Ln series. The region in which T_g is observable for this series is approximately the same as the one for the Al–Ni–Ln series, but its magnitude, that is, the magnitude of endothermic reaction, is smaller. As can be seen, the Al-based amorphous alloys in which T_g is present is limited to the three-element alloy series Al–TM–Ln where Ln may be any of the rare-earth metal elements, but TM denotes Ni and Co exclusively.

5. Effects of Added Elements on Magnitude of Glass Transition

Investigation of the effect of elements added with the view to increasing the magnitude of the endothermic reaction ΔH_g involved in the glass transition of the amorphous alloy series Al–Ni–Ln has led to the conclusion that the addition of small amounts of Co to the Al–Ni–Y series of alloys is effective. In the DSC curve of the amorphous alloy series Al–Ni–Y–Co in Figure 4, for example, replacement of Y by Co exclusively allows expansion of the magnitude of T_g. Figure 5, in turn, represents the range of compositions for the formation of the four-element amorphous alloy $Al_{95-x-y}Ni_5Y_xCo_6$ and the dependence

of its ΔH_g on relevant compositions. The ΔH_g is 43 J/mol for $Al_{85}Ni_5Y_{10}$, but increases with the growing amount of Co replacing Y and reaches the maximum 393 J/mol for $Al_{85}Ni_5Y_8Co_2$.

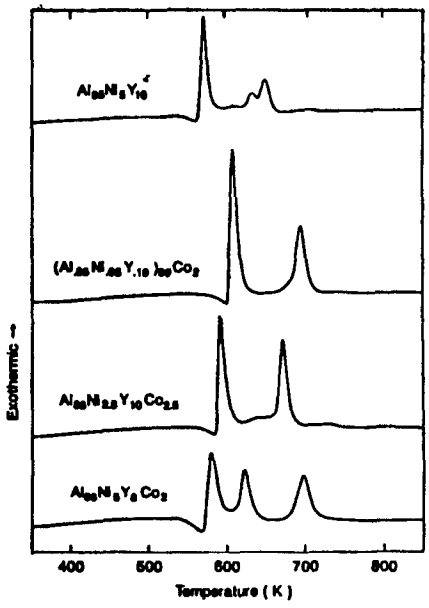

Figure 4. Dependence on Particle Diameters of X-Ray Diffraction Patterns for Powder of $Al_{85}Ni_{7.5}Mm_{7.5}$ Prepared by a Two-Step Rapid Cooling Method

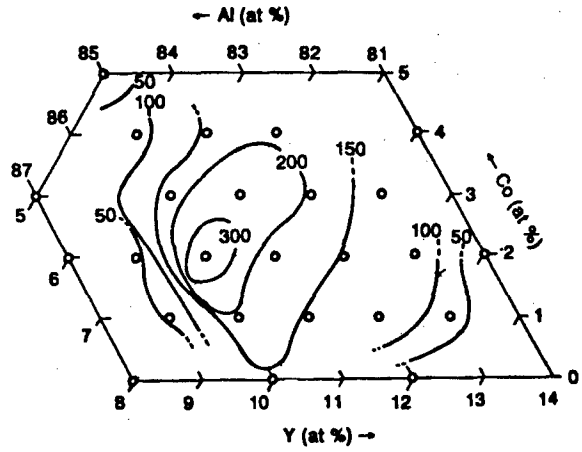

Figure 5. Dependence on Composition of Endothermic Heat of Glass Transition (ΔH_g) for Amorphous Alloy $Al_{95-x-y}Ni_5Y_xCo_y$

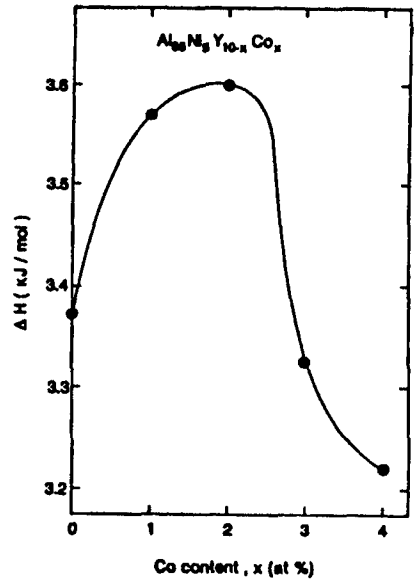

Figure 6. Dependence on Co Content of Exothermic Heat of Crystallization (ΔH_x) for Amorphous Alloy $Al_{85}Ni_5Y_{10-x}Co_x$

A replacement for Y by Co in amounts of 2~3 at.% for the amorphous alloy series Al-Ni-Y allows not only the ΔH_g to grow but also the exothermic heat of crystallization ΔH_x to increase notably. Figure 6 presents a plot of ΔH_x values (vs. Co content) for the alloy $Al_{85}Ni_5Y_{10-x}Co_x$; the value increases from 3.37 kJ/mol for $Al_{85}Ni_5Y_{10}$ to 3.57 kJ/mol for $Al_{85}Ni_5Y_8Co_2$. The ΔH_x represents the energy required for the transition from amorphous to crystalline structures and may conceivably grow when an amorphous phase or a supercooled liquid has its atoms packed in higher density and has them bound more strongly; the pronounced I in ΔH_g and ΔH_x of the alloy $Al_{85}Ni_5Y_8Co_2$, therefore, implies that replacement of Y by Co in small amounts allows the amorphous phase or the supercooled liquid to gain a high stability against development of growth of crystal nuclei.

6. Relationship Between the Magnitude of Glass Transition and the Critical Thickness of the Formed Amorphous Material

The R_c for formation of the amorphous phase falls with rising ΔT_x, as referred to above, and the magnitude of glass transition, in turn, rises notably with $Al_{85}Ni_5Y_8Co_2$, that is, with Co addition. These suggest the possibility of the alloy $Al_{85}Ni_5Y_8Co_2$ having a decreased R_c and allowing formation of ribbons in amorphous phase in increased thickness. The critical thickness for ribbons formed in the amorphous state, therefore, has been investigated by rapidly decreasing the rotating rate of the single roll and thus rapidly and continuously increasing the thickness of the ribbon; formation of a sticky amorphous material, up to some 250 μm, has been shown.[2]

The improved capacity for the formation of the amorphous phase for this four-element alloy was also confirmed by the increased maximum diameter gained from it. In cases where amorphous powders are prepared by 10-MPa-high-pressure gas atomization, the maximum diameter of the amorphous particles possible is some 25 μm for $Al_{85}Ni_5Y_{10}$, even with use of helium gas, whereas it is as high as 150 μm for $Al_{85}Ni_5Y_8Co_2$, allowing all particles to be amorphous.[3] When argon gas is used, the method still allows the amorphous phase in particles with a diameter below 25 μm.

7. Converted Glassifying Temperature and Capacity for Glass Formation

The dependence on the parameters ΔT_x and ΔH_g, which denotes the stability of supercooled liquid and the magnitude of glass transition, respectively, of the capacity for glass formation of alloys, was referred to above. In addition to these values, a smaller difference between T_m and T_g, that is, an increased ratio of T_g to T_m, may conceivably allow a larger capacity for glass formation of the alloy. Where the amorphous alloy series Al-Ni-Ln, in which T_m and T_g have actually been measured, are concerned,[1] the ratio T_g to T_m for $Al_{85}Ni_5Y_{10}$, for example, is 0.58 and the one for $Al_{85}Ni_5Y_8Co_2$ is an increased 0.61. An intimate correlation between the ratio and R_c for the amorphous-alloy formation has so far been shown for the metal series and calcogenide series of amorphous alloys.[4] On the basis of this correlation, the R_c of the former alloy is estimated to be 6.3×10^4~1.0×10^5K/s and that of the latter to be 8.1×10^3K/s. The extent of supercooling and the magnitude of R_c necessary for producing amorphous alloys thus falls in a large measure by a substitution of

Co for Y. Providing that the thermal conduction between the melt-paddle and the roll is conducted ideally in the single roll method of alloy production, there also exists a correlation between the ratio T_g to T_m and the maximum thickness X_c of the ribbon of the amorphous alloy produced,[4] allowing an estimate of X_c to be some 150 μm for the ratio of 0.59 and some 310 for the ratio of 0.61. This theoretical estimation agrees with the empirical results where amorphous single phase ribbons were some 150 μm in thickness for the former alloy and some 250 μm for the latter alloy.

8. Future Prospect

As discussed above, amorphous alloys based on Al are unique in terms of glass transition in that they exhibit a distinct transition point as opposed to those based on Fe, Co, Ni, and Ti, and they are also characteristic in that they have larger capacity for glass formation than Ti-based light alloys. Still many parts of the capacity for amorphous alloy formation and of physical properties of the amorphous state for the Al-based alloys remain unelucidated in comparison with those of the transition-metal alloys; hence, there seems to exist ample opportunity, as the research progresses, for finding a new Al-based amorphous alloy with a wider range for the supercooled liquid region and a greater capacity for the formation of amorphous alloy.

References

1. Inoue, A. and Masumoto, T., JOURNAL OF THE JAPAN INSTITUTE OF METALS, Vol 28 No 12, 1989.

2. Matsumoto, N., Inoue, A., and Masumoto, T., "The Abstract of the Lectures of the Japan Institute of Metals," September 1989, p 503; "Mater. Trans.," Japan Inst. Metals, being contributed.

3. Oguchi, M., Inoue, A., and Masumoto, T., not yet published, 1989.

4. Davies, H.A., "Amorphous Metallic Alloys," ed. F.E. Luborsky, Butterworths, London, 1983, p 8.

Preparation of Powder of Al Series of Amorphous Alloy

906C7531C Tokyo AL KEI AMORUFASU GOKIN NO KOZO TO TOKUSEI in Japanese 6 Feb 90 pp 9-12

[Article by Masahiro Oguchi, Teikoku Piston Ring Co., Ltd.]

[Text] **1. Introduction**

In recent years, Al-based amorphous alloys with a tensile strength as high as some 1,140 MPa together with a high corrosion resistance have been prepared from relevant Al-based alloys such as Al-Ni-Ln (rare earth element) by means of liquid quenching.[1,2] Later on, these alloys proved to undergo a distinct glass transition at a temperature lower than the temperature of crystallization T_x.[3] This glass transition phenomenon suggests that a bulky amorphous object, or amorphous bulk, may be produced with ease by solidifying a relevant alloy in the temperature region for supercooled liquid between its T_x and its glass transition temperature T_g and, therefore, the need for the amorphous alloy in large quantities.

The method for producing these alloy powders by rapid solidification includes the centrifugal spraying process, the rotating liquid atomization process, and mechanical milling of quenched ribbons, which, nevertheless, are not capable of producing the powder in large quantities. One method for preparing amorphous alloys in large quantities is gas-spraying, as Inoue, et al., have reported in the method of helium-gas high-pressure spraying.[4] The author, et al., attempted to prepare amorphous powder for Al-Ni-Ln alloys by application of argon-gas high-pressure spraying but found it extremely difficult to prepare the intended powder in single phase. It is important in the development of Al-based amorphous bulk from its amorphous powder that a technology be established for gas spraying or gas atomization for producing Al-based alloy powder in amorphous single phase, wherein Ar or N_2 is used instead of He.

Recently, the author, et al., successfully developed a new technology for rapid-quench solidification, wherein supercooled liquid drops having been produced by the high pressure Ar-gas spraying arc forced to collide with a rotating cooled object.[5] This method of liquid quenching in two steps has the advantage that it affords a cooling speed substantially higher than those of ordinary gas spraying methods because it involves quenching of supercooled

liquid particles and produces powder particles in the unique shapes of old oval Japanese gold coins and of thickness 1~3 μm.[5-7] Application of this two-step liquid quenching method may conceivably allow preparation of amorphous alloys of the Al-Ni-Mm series even with use of Ar instead of He. This article deals with the trial manufacture of amorphous alloy powders of Al-Ni-Mm (Mm: misch metal) and Al-Fe-Mm series by the above two-step method and with a comparison of the products in terms of their microstructures and shapes with those by ordinary high-pressure gas spraying methods.[8-10]

2. Method of Experiment

Alloys with the composition $Al_{84-85}Ni_{7.5-10}Mm_{6-7.5}$ (in at.%) and $Al_{85}Fe_{7.5}Mm_{7.5}$ whose liquid-quenched or melt-spun ribbons exhibit high tensile strength and high toughness were used in the experiment. The parent alloys were dissolved in a radio frequency furnace under Ar and cast into a copper die with a 15 mm diameter. For preparing the powder, some 200 grams of the parent alloy was packed into a crucible for spraying use, redissolved under Ar, and subsequently subjected to treatment with an apparatus, as shown in Figure 1, which combines high-pressure gas-spraying and centrifugal quenching to give the product. The supercooled spherical liquid drops produced therein by the high-pressure gas spraying were subsequently allowed to collide with a rotating cooled cone set just under the nozzle, leading to formation of flat particles with a large aspect ratio and limited thickness. The rotating cooled cone was made of copper and had a diameter of 200 mm and a height of 70 mm. Through the nozzle, which had a diameter of 4 mm, was spurted the Ar gas at a pressure of 9 MPa. The grain size distribution was investigated by laser diffraction (Microtrace 7995-10SRA) and the grain sorted out according to size with sieves. X-ray diffraction, scanning electron microscope (SEM), and optical microscopy were used to study the microstructures and shapes of the particle for each size group, and differential scan calorimetry (DSC) adopted for investigating thermal stability.

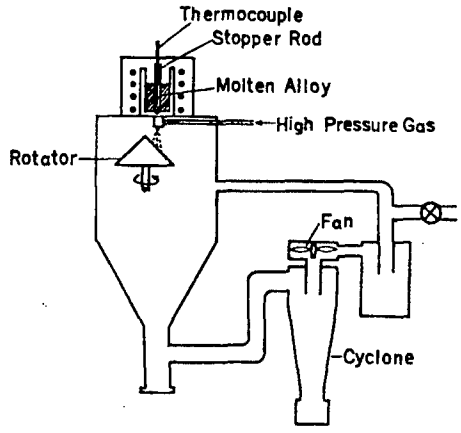

Figure 1. Diagram of Two-Step Liquid Quench Apparatus

3. Preparation of Spherical-Particle Powder by a High-Pressure Argon-Gas Atomization or Spraying

The shapes and microstructures produced by ordinary high-pressure Ar-gas spraying was investigated in order to compare them with those prepared by the two-step liquid quench method. Figure 2 [not reproduced] presents the shape and the cross-section microstructure of the powder particles of $Al_{85}Ni_{7.5}Mm_{7.5}$ atomized by Ar-gas spray and below 20 μm in particle size. The particle, being spherical in shape, has a smooth surface in cases where its size is below some 5 μm, but uneven where the size is above that. Optical microscopic observation also distinctly confirmed contrastive crystal phases present for particles of size above some 5 μm,1 but no such phases for those of size below that value, thereby indicating single amorphous phase in structure in the latter case. An investigation of changes, with grain size, of X-ray diffraction patterns for the powder of the above alloy proved that no pattern group was found in which the amorphous phase occurs in all grain-classes, and that peaks of Al, triclinic Al_4 (La, Ce), and Al_3Ni compound were demonstrable, that is, it became evident that the formation of spherical amorphous particles of the above alloy by the ordinary high-pressure Ar-gas spraying method is limited to particles of sizes below 5 μm.

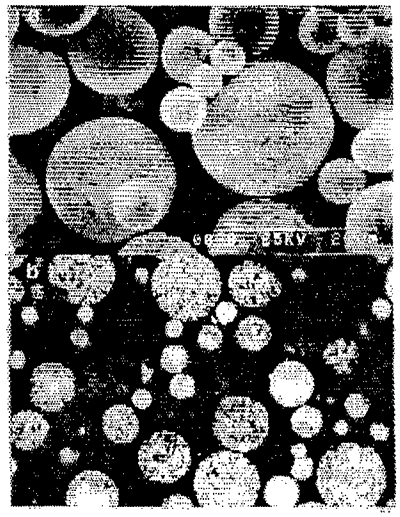

Figure 2. Microstructures, as Observed by SEM and by Optical Microscope for Alloy Powder and Its Cross Section, Respectively, of $Al_{85}Ni_{7.5}Mm_{7.5}$ of Size Below 20 μm Produced by High-Pressure Argon Gas Spraying

4. Preparation of Flat-Particle Powder by the Two-Step Liquid Quench Method

The grain-size distribution for the powder produced by the two-step liquid quench was different from the one for the powder formed by the ordinary high-pressure gas spraying. In the latter case, the number of particles was largest in particles of size below 25 μm, and close to zero in particles of size from 63~75 μm, whereas in the former the particles exhibited approximately equivalent frequency over the wide range of 25~150 μm. This difference in grain-size distribution was attributable in the former case, to the particles

of sizes above 63 μm cooling with the rotating cooled cone and becoming flattened. Distribution of particles with a size below 25 μm, however, were nearly identical for the two cases, which suggests that small liquid drops produced by the quenching of the first step in the former case had a kinetic energy so poor that their advancement was disturbed by the current caused by the cone rotating at high speeds and that they thus fail to reach the cone. Figure 3 presents shapes and surface conditions of the relevant alloy produced by the two-step liquid quench. The shape was spherical for particles of size below 25 μm, but flat and about 1~3 μm in thickness for those of a larger size, indicating that solidification of particles of size 25~90 μm occurred by the collision of the sprayed liquid drops with the rotating cone. The particle had a large aspect ratio of some 30~100 and its surface was fairly smooth.

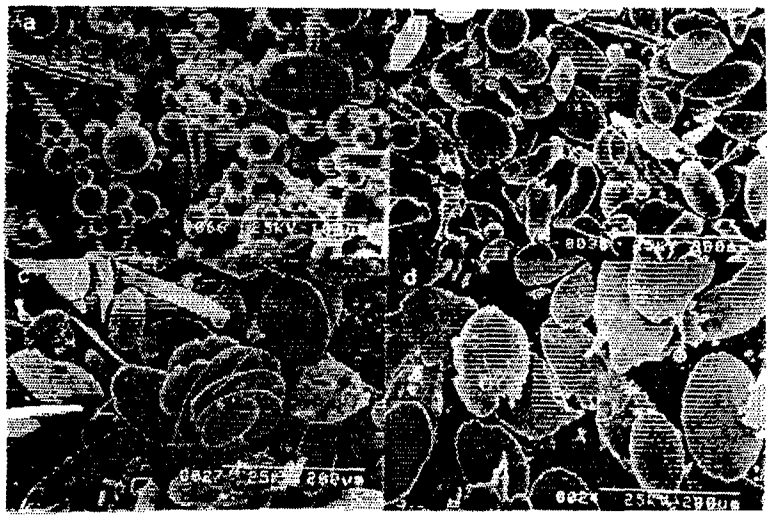

Figure 3. Microstructure, as Observed by SEM, of the Alloy Powder $Al_{85}Ni_{7.5}Mm_{7.5}$ Produced by the Two-Step Liquid Quench Method

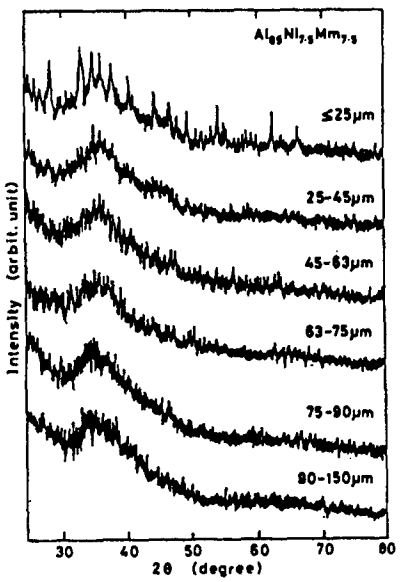

Figure 4. X-Ray Diffraction Patterns of the Alloy $Al_{85}Ni_{7.5}Mm_{7.5}$ Which Was Produced by Two-Step Liquid Quench Method and Which Varied With Grain Size

Figure 4 presents changes of X-ray diffraction patterns with varying grain diameter for particles of this alloy produced by the two-step liquid quench. Evidently, the flat particles of size 25~150 μm exhibited amorphous structures, but the spherical ones of size below 25 μm had the amorphous phase and the crystalline phase (Al + Al_4(La, Ce) + Al_3Ni) intermingled in the pattern; the nonequilibrium phase involving the amorphous phase was thus formed exclusively in flat particles of the powder prepared by the two-step quench. Figure 5 shows the temperature for starting crystallization T_x, (the temperature for glass transition) T_g, crystallization peak temperatures T_{p1}, T_{p2}, and T_{p3}, and ΔH_x for varying grain diameter. The spherical particles did not exhibit the glass transition phenomenon, but the flat ones did distinctly, with T_g being stationary for different grain diameters. The amorphous particles of size above 25 μm underwent three stages of exothermic reaction to give a crystalline phase with the ΔH_x standing at 3.1 kJ/mol for 45~63 μm particles and at 3.0 kJ for 75~90 μm particles and thus exhibiting no appreciable changes for different particle sizes. The two exothermic-reaction peaks on the lower temperature side were ascribed to the deposition of Al_4(La, Ce), Al_3Ni, and an unidentified X phase, and the one of low intensity on the high temperature side was to the transformation of the X phase into Al, Al_4(La, Ce), and Al_3Ni. This crystallization process agreed with the spherical powder-particles resulting from the Ar-gas spraying being composed of Al, Al_4(La, Ce), and Al_3Ni phases.

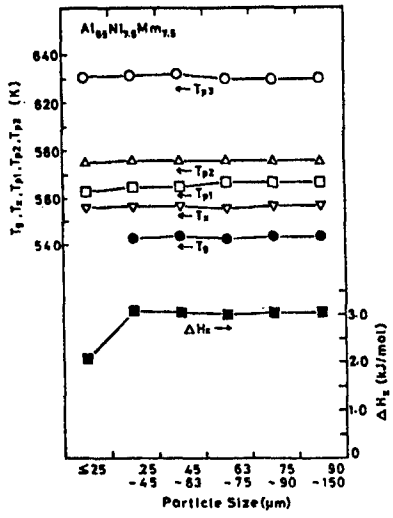

Figure 5. Particles of Grain Diameter Vs. Temperature of Glass Transition T_g, Temperature of Starting Crystallization T_x, Temperatures of Crystallization Peaks T_{p1}, T_{p2}, and T_{p3}, and Amount of Exothermic Heat Due to Crystallization

5. Improvement of the Amorphous Transformation by Means of a Supercooled Liquid Quench

Unlike the powder of the alloy Al-Ni-Mm produced by the ordinary high-pressure Ar-gas spraying, wherein particles of size below 5 μm exclusively are amorphous, the one prepared by the two-step liquid quench method may be made to have (amorphous) particles in thickness of 2~3 μm for all different

particle sizes, indicating that the cooling speed was notably raised by the relevant method. Two factors conceivably attributable to increased cooling speed are the following: One is the re-cooling of the liquid drops that have been cooled to temperatures below its melting point by the high-pressure Ar-gas spraying. Figure 6 presents a diagram showing cooling curves for the powders of different particle diameters produced by the two-step liquid quench compared with those by the ordinary one-step high-pressure gas spraying. Curves (a) and (b) represent the behavior in cooling of spherical particles of sizes below 5 μm and between 5 and 20 μm, respectively. The particles of size below 5 μm are afforded a high cooling rate because of its limited volume and the amorphous state, whereas the liquid drops of size between 5 and 20 μm are turned into a crystalline state in the first step of cooling because they have insufficient kinetic energy to have effective collisions with the rotating cone. The spherical particles of size above 25 μm, in turn possess a high kinetic energy because of their large volume and thus collide effectively with the rotating cooling cone, leading to formation of flat particles in thickness of 2~3 μm, as curve C shows. The other factor is the thinness of particles and resulting large surfaces of contact to the roll of the flat particles. Another conceivable factor is that the liquid drops just following the spraying have a flying speed as high as 500~1,000 m/s,[11] which may enhance the contacting condition of the particle and hence the cooling effect by thermal conduction.

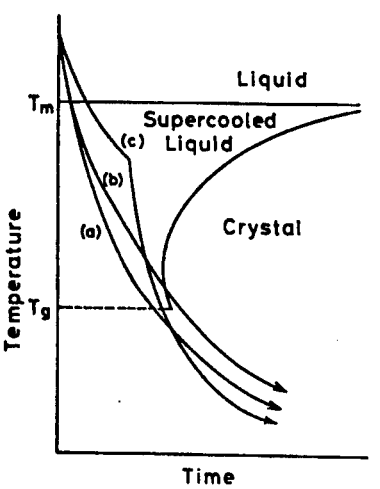

Figure 6. Diagram for Changes With Time of Temperature of Liquid Drops Being Cooled by Two-Step Liquid Quench Method for Different Liquid-Drop Sizes

6. Conclusion

The two-step liquid quench method, which allows supercooled fine liquid drops to collide with a rotating cone, yielded powder particles of the alloy $Al_{85}Ni_{7.5}Mm_{7.5}$ in the shape of old Japanese gold coins about 1~3 μm in thickness for particles of sizes above 25 μm. Whereas powder particles of this flat type and those of sizes below 5 μm in spherical shape had crystalline phases of Al, Al_3Ni, and Al_4(La, Ce). This two-step method is available for the preparation of an Al-based amorphous powder characterized by a large aspect ratio, thinness, and a unique shape and, hence, its prospect is very bright.

Acknowledgement: The present article is a summary of the result of research achieved during the author's stay as a researcher at the Research Institute for Iron, Steel, and Other Metals, Tohoku University, and the author expresses his deep gratitude for the tremendous guidance rendered by Professor Takeshi Masumoto and Associate Professor Akihisa Inoue.

References

1. Inoue, A., Ohtera, K., Tsai, A.P., and Masumoto, T., JPN. J. APPL. PHYS., Vol 27, 1988, p L479.

2. Ibid., Int. Meeting on Advanced Materials, Materials Research Society, 1988, in press.

3. Inoue, A., Ohtera, K., Tsai, A.P., Kimura, H.M., and Masumoto, T., JPN. J. APPL. PHYS., Vol 27, 1988, p L1579.

4. Inoue, A., Kita, K., Ohtera, K., Kimura, H.M., and Masumoto, T., J. MATER. SCI. LETT., Vol 7, 1988, p 1287.

5. Inoue, A., Komura, T., Saida, J., Oguchi, M., Kimura, H.M., and Masumoto, T., INT. J. RAPID SOLIDIFICATION, Vol 4 No 3, 1989, p 181.

6. Inoue, A., Saida, J., and Masumoto, T., MATER. TRANS., Japan Inst. Metals, Vol 30, 1989, p 291.

7. Inoue, A., Saida, J., Tachiya, Y., Tsai, A.P., and Masumoto, T., Int. Meeting on Advanced Materials, Materials Research Society, Tokyo, May 1988, in press.

8. Oguchi, Yamaguchi, Harakawa, Inoue, and Masumoto, Summary of lectures at meeting of the Japan Institute of Metals, Spring 1989, p 44.

9. Oguchi, Yamaguchi, Inoue, and Masumoto, Proceedings of lecture series of the Japan Institute of Metals, Fall 1989, p 504.

10. Inoue, A., Oguchi, M., Yamaguchi, H., and Masumoto, T., MATER. TRANS., Japan Inst. Metals, Vol 30, 1989, p 12.

11. Liu, J., Arnberg, L., Backstrom, N., Klang, H., and Savage, S., POWDER MET., Powder Met. Inst., Vol 20, 1988, p 17.

Molding of Al Series Amorphous Alloy

906C7531D Tokyo AL KEI AMORUFASU GOKIN NO KOZO TO TOKUSEI in Japanese 6 Feb 90 pp 13-16

[Article by Takeshi Masumoto, Research Institute for Iron, Steel and Other Metals, Tohoku University]

[Text] **1. Introduction**

The amorphous alloy of Al series discovered by the author, et al., in 1988 is a marvelous material with a tensile strength of more than 120 kg/mm^2 and with a specific strength about double that of the super-Duralumin currently available.[1] Nevertheless, the alloy is available in the form of ribbons, thin wires, or powders of limited mass only, since it is produced by liquid quench, and its application, therefore, is also limited to components of small size. It is necessary to produce the alloy in the form of boards and round rods of large size if its strength is to be made available effectively.

An amorphous alloy, upon heating, is transformed into crystal and loses its characteristics since it is in a semistable state. It, therefore, needs to be molded at low temperature if it is to be solidified and still maintain its amorphous state intact after the molding; namely, methods and conditions for its molding need to be investigated and devised. One method available for this purpose is the dynamic process using a shock wave, including the Flyer method, and explosive cladding; another is the static process based on application of pressure, including hot pressing, hot isostatic pressing (HIP), extrusion, and rolling. The present lecture deals with the basic concept of the molding of amorphous alloy of Al series by means of the latter period, the static process.

2. Important Factors in the Solidification of Amorphous Alloys

(1) Crystallization Temperature and Glass Transition Point

A major factor in solidifying and molding amorphous alloy into a solid shaped object is the stability of the material. Figure 1 presents changes in volume of an amorphous alloy upon heating. Application of heat to a quenched amorphous material first allows relaxation of the structure at a low

temperature and then deposition of crystals at T_x, the temperature of crystallization, in most of the cases. In some very limited cases, for example, in the series Pd-Cu-Si, Pd-Ni-P, and Pt-Ni-P, however, the amorphous solid is first transformed into supercooled liquid and then undergoes crystallization; namely, a distinct glass transition point shows up in the plot.

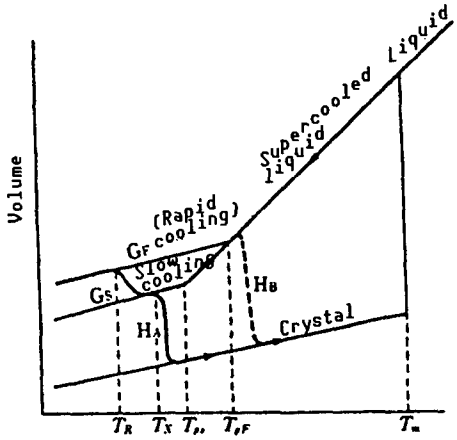

Figure 1. Diagram Qualitatively Illustrating the Change of an Amorphous Phase by Heating

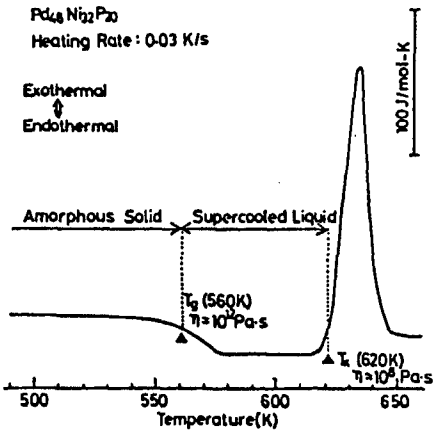

Figure 2. DSC Curve for the Amorphous Alloy Pd-Ni-P

Figure 2 presents the differential scan calorimetry (DSC) curve of $Pd_{48}Ni_{32}P_{20}$, a representative amorphous alloy exhibiting a distinct T_g. The alloy, with a T_g of 560 K and a T_x of 620 K, allows supercooled liquid to form in the T_x-T_g range of 60 K.

(2) Transformation Into the Amorphous State and Critical Cooling Temperature

A 100 percent amorphous alloy powder needs to be used if it is to be molded and, hence, an alloy composition amenable to transformation into the amorphous state needs to be selected. A well-known measure for estimating the ease with which a material can be turned into the amorphous state is the critical cooling rate. Figure 3 shows the relationship between the crystallization starting curve and the cooling curve for liquids. The critical cooling rate of alloy A in the figure is represented by R_C^A, tangent to the nose of curve C, and that for alloy B by R_C^B, which implies that alloy A needs to be cooled more quickly to give good amorphous phase.

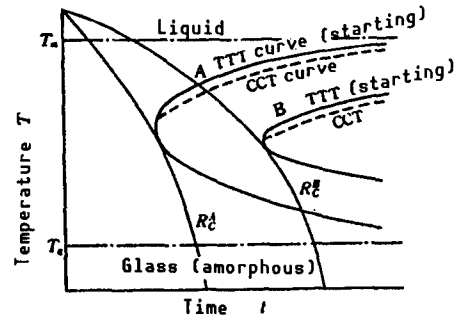

Figure 3. Crystallization From Liquid and Critical Cooling Rate

The cooling rate, as is known, is generally related to the ratio T_g/T_m, a conversion formula for temperature. Ordinary oxide-glasses, located in a region as shown in Figure 4, allow cooling to go on at a slow rate without precipitating crystals, whereas alloys undergo crystallization unless the rate is sufficiently large. Alloys involving Fe, Co, Ni, etc., as the major constituent, in particular, need as high a rate as 10^5~10^6/s, and those with noble metals such as Pd and Pt contained as the principal component require a rather small rate of 10^3~10^4/s. As described below, alloys with a smaller critical cooling rate, that is, those with its C curve located on the longer-time side of Figure 3, are subjected to solidification with more ease and, hence, selection of alloys with a larger T_g/T_m ratio is important.

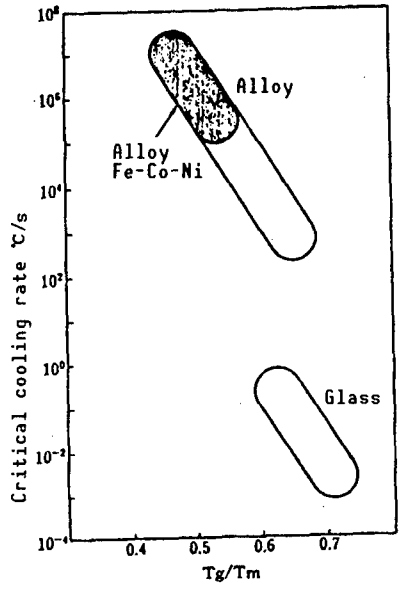

Figure 4. Relationship Between the Critical Cooling Rate and the Ratio T_g/T_m

(3) Condition for Solidification (Temperature, time, pressure)

If an amorphous alloy powder is to be subjected to solidification and molding while its amorphous state is being preserved intact, the conditions of processing time, temperature, and pressure need to be under control. In qualitative terms, the process needs to be performed in a shorter time-lower temperature region, below the TTT curve as shown in Figure 5. In the figure, the processing condition grows easier as the TTT curve approaches closer to the long-time side. It is also necessary to learn how pressure affects the crystallization, since conditions for the treatment time and temperature may grow more stringent if a rising pressure enhances crystallization. With the view to investigating this effect of pressure, an experiment for hot pressing of the alloy Pd-Ni-P was carried out[2]; as seen in Figure 6, crystallization temperature T_x rose linearly with increasing pressure applied at about a rate of 15 K/1 GPa. This implies that pressure application inhibits crystallization, and thus stabilizes the amorphous state, and that, by shifting the TTT curve to the long-time side, improves the treatment condition for solidification and molding.

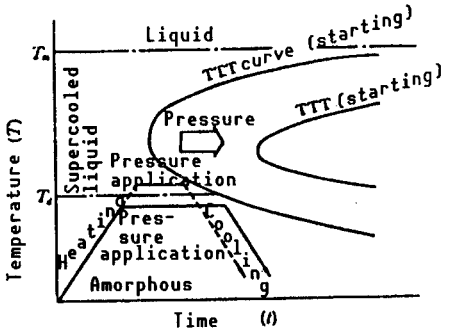

Figure 5. Diagram for Relationship Between TTT Curve and Conditions for Thermal Treatment in Sintering Amorphous Alloy Powders

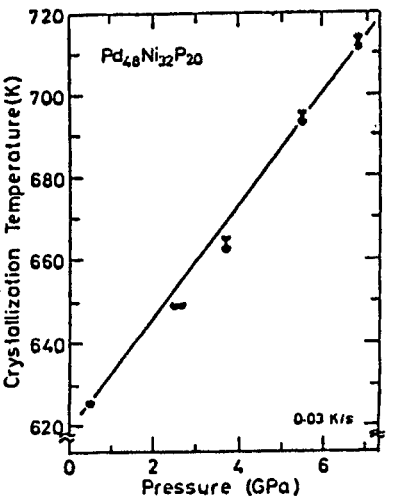

Figure 6. Effect of Pressure on T_x for Amorphous Alloy Pd–Ni–P

(4) Conditions for Compacting the Powder

Results of testing on spherical particles of the powder of the alloy $P_{48}Ni_{32}P_{20}$ for the effects of the three factors, namely, the temperature during pressure application T_p, the level of the pressure P, and the period of the pressure application T_p on the compacted states, are summarized as follows[2]:

1) The viscosity coefficient varied from 10^{12}Pa·s at T_g of 560 K to 10^{8}Pa·s at T_x of 620 K, and application of pressure at a temperature just below T_x allowed a density as high as about 99.8 percent.

2) Compaction is sensitively affected by T_p, but rather not by t_p and P.

3) The viscosity coefficient of a supercooled liquid under pressure rises at temperatures above T_g, and does so pronouncedly as the T_p rises.

4) Crystallization is inhibited by pressurization; the alloy does not precipitate crystals after heating for 3 hours, providing a pressure of 630 MPa is applied.

5) A multiple-step treatment, wherein the alloy is subjected to repeated treatments of pressurization heating, allows compaction at low temperatures.

3. Solidification and Molding of Al Series of Amorphous Alloy Powder

(1) Dictating Factors in Solidification and Molding

The author, et al., discovered the three-element amorphous alloys of Al series, Al–M–R·E, where M denotes metals including Fe, Co, Ni, and Cu, and R·E

denotes rare earth metals including Y, La, and Ce.[1] Of these, the Al–Ni–R·E series turns into the amorphous state most readily and T_g is distinctly present in some of them.3 For example, shown in Figure 7 are the range of formation of amorphous alloys and the range of T_g for the series Al–Ni–Y. The alloy $Al_{85}Ni_5Y_{10}$, for example, has a T_g of 510 K, T_x of 560 K and, hence, a T_x–T_g of 50 K, which roughly represents the range of the supercooled liquid state. The ratio T_g/T_x stands at some 6.0, and hence an estimated critical cooling rate of about (10^4)°C/s. These values are smaller than those for the Fe, Co, and Ni series by a factor of some 10, which indicates that the Al series of alloys are amenable to amorphous formation and to solidification and molding.

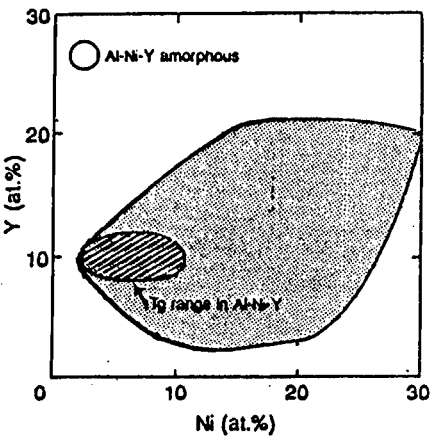

Figure 7. Range of Composition for Amorphous Alloy Pd–Ni–P

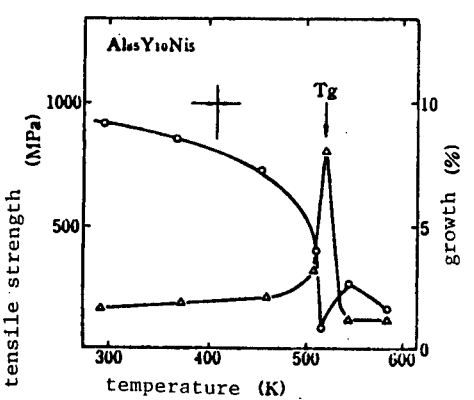

Figure 8. Dependence on Temperature of Tensile Strength and Elongation for the Alloy Al–Ni–Y (5 minutes heating)

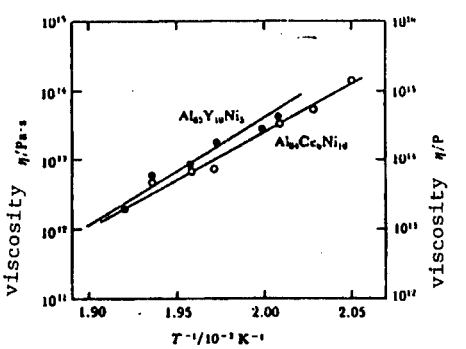

Figure 9. Dependence on Temperature of Viscosity for the Alloy Al–Ni–Y

Figure 8 presents the dependence on temperature of the tensile strength and elongation of the alloy,[3] which shows a pronounced increase in elongation in the vicinity of T_g. Presented in Figure 9 is the viscosity of the alloy as estimated by the dependence on temperature of the elongation of the alloy under a 5-gram load, which varies from 10^{12}~10^{14}Pa·s over the range of T_g–T_x, values near equivalent to those for the amorphous alloy series Pd–Ni–P.

(2) Method of Solidification and Feature of Solidified Materials

Amorphous particles with a diameter below 25 μm were prepared by means of a high-pressure He gas spray from the alloy $Al_{85}Y_{10}Ni_5$, which showed distinct T_g and subsequently subjected to hot pressing at a temperature near its T_g of 550 K, under a pressure of 980 MPa for 30 minutes. The resulting solid had a density of more than 99 percent.[4] Solids of still higher density were afforded when the material was subjected to a warm extrusion, where higher shear strengths work (Figure 10).[5]

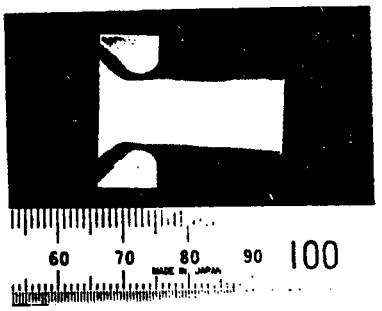

Figure 10. External Appearance of Materials Subjected to Warm Extrusion

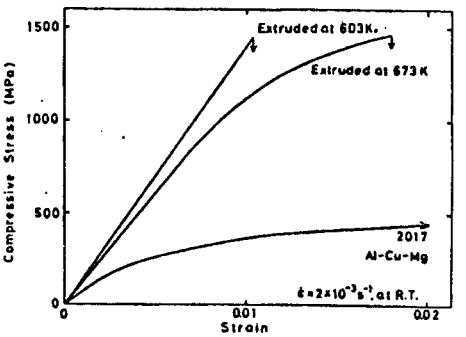

Figure 11. Plot of Compressive Stress Vs. Strain (Elongation) for Extruded Material Al-Y-Ni

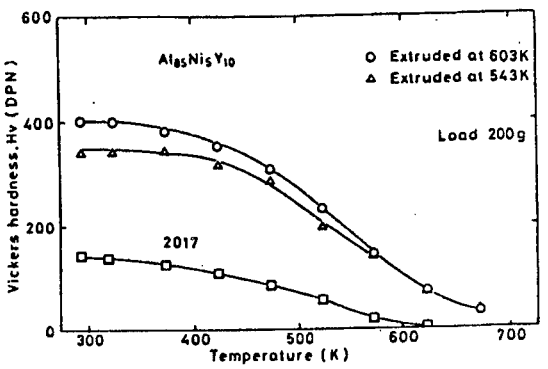

Figure 12. Hardness Characteristics at High Temperature for Extruded Material Al-Y-Ni

The dependence on temperature of compression strength and hardness of the product having been subjected to the warm extrusion are presented in Figures 11 and 12, where the products prepared by extrusion at 543 K, 603 K, and 673 K were made up of amorphous single phase crystals partly mixed with the amorphous phase, and entirely crystals, respectively. The solid materials also exhibited superior mechanical properties.

References

1. Inoue, A., Ohtera, K., Tsai, A.P., and Masumoto, T., JPN. J. APPL. PHYS., Vol 27, 1988, p L280.

2. Yamamoto, T., Master's Degree Thesis, 1987, Postgraduate Engineering Course of Tohoku University.

3. Inoue, A., Ohtera, K., Tsai, A.P., Kimura, H.M., and Masumoto, T., JPN. J. APPL. PHYS., Vol 27, 1988, p L1579.

4. Inoue, A., Kita, K., Ohtera, K., and Masumoto, T., J. MATER. SCI. LETT., Vol 7, 1988, p 1287.

5. Inoue, A., Masumoto, T., Ohtera, K., and Kita, K., Proc. 1st Japan Inter. SAMPE Sympo, 1989, p L7.

X-Ray Analysis of Structure for Few Al-Based Amorphous Alloys

906C7531E Tokyo AL KEI AMORUFASU GOKIN NO KOZO TO TOKUSEI in Japanese 6 Feb 90 pp 17-20

[Article by Yoshio Waseda, Institute for Research of Beneficiation and Smelting, Tohoku University]

[Text] **1. Introduction**

Of the amorphous alloys produced by the liquid quench method, some have undergone successful development and are finding practical applications in electronic components, composite materials, and functional materials. However, even in the 1970s, when research on amorphous alloys had become widespread, the report of results of research on Al-based amorphous alloys was scarce, although available,[1] in comparison with research on Fe-based amorphous alloys. The quasicrystal boom resulting from a report in the fall of 1984 on a quenched Al-Mn alloy, of "an electron beam diffraction pattern pointing up the presence of a five-fold-symmetric-axis orientation order regarded as incompatible with the periodic nature of crystals,[2]" and, more recently, the discovery of an amorphous alloy of Al-Y-Ni exhibiting mechanical properties surpassing those of Duralumin, the reputed alloy of highest strength,[3] triggered resumption of research of Al-based amorphous alloys, with an urgent desire for the characterization of the structures of these comparatively new Al-based alloys. Of the various means for relevant structural analysis available, X-ray diffraction still is important.

The present report is concerned with results of a structure analysis for some of the Al-based amorphous alloys conducted by means of X-ray diffraction, including that of abnormal scattering.

2. Feature of Environmental Structure Analysis by Means of Radial Distribution Function and Abnormal X-Ray Scattering

In the research of a material series that does not exhibit a periodic atomic arrangement, as in crystals, the radial distribution function is used as a measure of the probability of finding other atoms at a given distance from a given atom or as a measure of the shift from the chaotic distribution of the average atomic density at a given distance from the atom.[4] Where the incident X-ray energy is close to that of the absorption edge of the relevant element,

each element has its own intrinsic absorption edge; in turn, the scattering power of of the X-ray is not to be represented by the usual f^0 term alone that is independent of the incident X-ray energy, but one also needs to allow for the terms f' and f"--referred to as the anomalous dispersion terms--that are dependent in a large measure on the incident X-ray energy,[5] as given by the formula

$$f(Q,E) = f^o(Q) + f'(E) + if"(E)$$

where Q denotes the wave vector and E the incident X-ray energy. In general, fine structures corresponding to the extended X-ray absorption fine structure (EXAFS) and XANES signals appear on the high-energy side of the absorption edge, whereas the abnormal X-ray scattering, AXS, is related to the above two signals complementarily as a means of structure analysis and available on the low-energy side of the edge where the imaginary part of the anomalous dispersion term f" is small and stays nearly constant and real part f' alone exhibits acute sharp changes.

Structural analyses based on AXS do not require phase shift data and other parameters, unlike those by EXAFS, etc., and basic procedures so far established are available with little modification. The analysis also characteristically allows an estimation, as a function of distance, of the environmental structure surrounding an atom in question in a polycomponent system, even in cases where the atomic numbers of the relevant atoms differ only by one--atoms being generally several hundred eV or more apart and regarded as hardly amenable to X-ray--since measurement of the dependence on energy of AXS intensity is only in the 200~300 eV range.[6] This environmental analysis is available whether the material in question is crystalline or amorphous and is particularly useful in the case of polycomponent amorphous materials where average information alone hardly allows satisfactory interpretation because of mingling of information of many component pairs.

3. Example of Analysis for the Alloys Al-Mn-Ge and Al-Ge-Ni

Whereas the two-element alloy Al-Mn does not give a single amorphous phase by quenching, addition of a third element, such as Ge or Si, allows yielding of the phase with comparative ease. Of the research on the three-component Al-based amorphous alloys produced on the basis of such properties, some results for the structural analysis of the alloy Al-Mn-Ge are given below.

Figure 1 presents X-ray scattering intensity curves for the alloys $Al_{60}Mn_{10}Ge_{30}$ and $Al_{60}Mn_{20}Ge_{20}$. The curve for the former alloy represents the feature of typical amorphous alloys and is made up of a large, comparatively sharp peak followed by a few small peaks. The first peak is divided into three, a behavior that has not been observed to date and is unique to this alloy. In this connection, the phenomenon of the first peak being divided into two has often been observed in alloys of which the constituents differ much from each other in dimension, among other things. The latter alloy, in turn, presents a sharp peak which, by use of the method of Bancel, et al., is attributable to the icosahedral phase of the alloy.[7] As indicated in the figure, agreements are notable in the position of peaks, etc., between the X-ray scattering intensity

curve of an amorphous alloy and that of relevant quasicrystals, suggesting that amorphous alloys involve a short-range regularity in structure whose structural elements are similar to those of quasicrystals; this implies that this short-range structural regularity is different from those observed in chaotic distribution.

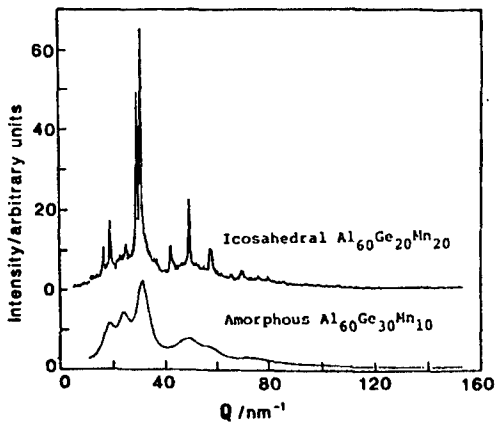

Figure 1. X-Ray Scattering Intensity Curves (Plots of X-ray scattering intensity vs. wave vector) for Quasi-Crystal and Amorphous Alloys Al-Ge-Mn

The splitting of the first peak observed in the Al-Mn-Ge series of amorphous alloy was also reported in other Al-based amorphous alloys, including those of Al-Ge-Ni series, although details of the latter were different from those of the former. In this connection, the possibility of the existence of two phases involving special components in high concentrations has been pointed out on the basis of results of not only relevant X-ray diffraction patterns but also of electron microscopy observation and others. It is conceivable that differences in the environmental structure surrounding an element at issue is present even in the amorphous phase, providing relevant materials have shifted in a large measure from the characteristic "chaotic distribution and homogeneity" of that phase and approached the state of coexistence of two phases. Results of experiments, as based on this point of view and where abnormal X-ray scattering was examined for the amorphous alloy $Al_{60}Ge_{30}Ni_{10}$ by using the K absorption edges of Ge and Ni, are presented in Figures 2 and 3.[8] It is evident from the result that an extremely contrastive dependence on energy of the scattering intensity is present; the environmental structure function for Ge reflecting the correlations between the pairs of Ge and Ge, Ge and Al, and Ge and Ni may be taken basically as representing an amorphous state (Figure 2); the one for Ni reflecting the correlations between the pairs of Ni and Ni, Ni and Al, and Ni and Ge, however, shows characteristically sharp positive and negative peaks (Figure 3). The structural factor of amorphous systems (crystalline systems of chaotic distribution) is basically of chaotic distribution and runs proportionally to an average atomic scattering factor, which may be denoted as $c_Af_A+cBf_B+\cdots$. The abnormal X-ray scattering intensity, therefore, takes positive values in every wave vector. Nevertheless, as is well known in the case of superlattices, etc., a particular scattering peak corresponding to a pronounced regularity in structure involves the term denoted by f_B-f_A and, hence, in cases where a

substantial regular region is present in the systems in question, the abnormal X-ray scattering intensity patterns probably may not take a positive value at all wave vectors, but exhibit both positive and negative values in their peak profile. The environmental structure function for Ni seeks to fall into the latter case. Although it is still difficult to elicit quantitative information on the regular region of the relevant function for Ni from the results shown in Figure 3 alone; the solution to this problem is left for the future. Nevertheless, the homogeneity in the distribution of Ni atoms conceivably overweighs the inhomogeneity therein, providing relevant values are averaged in the entire system, and the alloy, therefore, must fall into the category of amorphous materials.

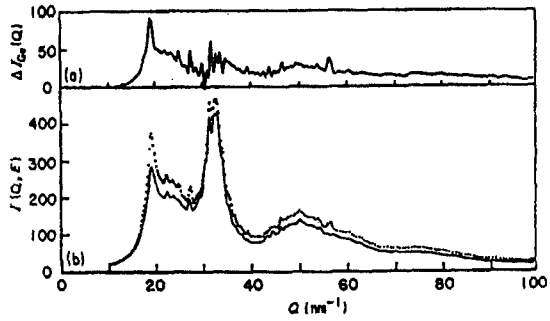

Figure 2. Environmental Structural Function of Amorphous Alloy $Al_{60}Ge_{30}Ni_{10}$ With Respect to Ge

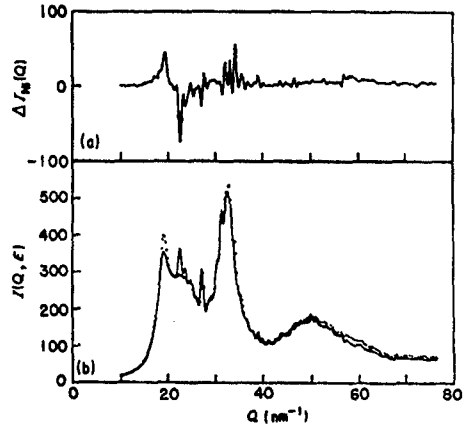

Figure 3. Environmental Structural Function of Amorphous Alloy $Al_{60}Ge_{30}Ni_{10}$ With Respect to Ni

4. Examples of Analysis for Al-Y and Al-Y-Ni Alloys

With Al-based amorphous alloys involving Ni and Y having been found to possess mechanical properties far surpassing those of Duralumin,[3] attention has been focused not only on their application as raw materials but also on elucidation of the mechanism by which these excellent properties are to emerge. A trial X-ray structure analysis for the amorphous alloys $Al_{90}Y_{10}$ and $Al_{87}Y_8Ni_5$ by use of the K edge of Y was, therefore, conducted in order to gain clues to the question at issue, and results thus obtained follow.[9]

Figure 4 presents the environmental structural function of the alloy $Al_{90}Y_{10}$. In the region of 0~13 nm^{-1} of Q, a distinct prepeak is notable, which suggests the presence of a comparatively large local structure and which is also notable in measurement data for the abnormal X-ray scattering (AXS) using the K absorption edge of Y. The well-known empirical formula based on many empirical results $Q \cdot r = 2\pi$ holds for the relationship between the relative distance r, as noted in the amorphous state of alloys and other materials, and the peak position Q found in the scattering intensity curve. It may be inferred from this formula that the prepeak in the region of 0~13 nm^{-1} of Q suggests the presence of a local structural unit of size 0.60 nm^{-1}. The environmental structural function of the alloy $Al_{87}Y_8Ni_5$, in turn, is presented

in Figure 5. It can be readily seen that the function of this alloy, including the prepeak observed in the region of 0~13 nm^{-1} of Q, is similar to that of the alloy $Al_{90}Y_{10}$. The radial distribution function, RDF, computed from results of Figures 4 and 5 are presented in Figure 6. The environmental RDF for Y, in this connection, does not include the correlations Al–Al, Al–Ni, and Ni–Ni. The number of coordinations calculated from areas on the assumption that the atomic correlations for the peaks are Gaussian is shown in summary in Table 1. It can be seen from the table that the contribution from the Y–Y correlation is limited and that atoms surrounding a Y atom are mostly Al, although they include also some Ni. The share of different atoms surrounding an Al atom are 82, 14, and 4 percent for Al, Y, and Ni, respectively; the share of Al is smaller than the ones predicted from the relevant compositions, and that of Y larger with that of Ni unchanged, which is an experimental result suggesting that the correlation Al–Y is stronger than those of the other pairs in this Al-based amorphous alloy. The phase diagrams of the two two-element alloys Al–Y and A–Ni exhibit merely a very shallow eutectic point precluding any high capacity of the two alloys for the formation of amorphous alloys. In the three-element alloy Al–Ni–Y, in turn, the characteristic correlations among the constituting elements, as studied above, allows the alloy to form a local structure of comparatively strong bonding and thus to be prevented from a rearrangement of its atoms into a crystalline phase at the time of rapid cooling and solidification, which instead, conceivably leads to formation of an amorphous phase with comparative ease. The environmental structural function using an Ni absorption edge, in this connection, has indicated a positive correlation in principle over all of the wave vector range, as in the case represented by Figure 2,[9] suggesting a uniform distribution of Ni throughout the alloy. The excellent mechanical properties of the new Al-based three-element amorphous alloy Al–Y–Ni may conceivably be the result of the three-element alloy, as seen above, having the two element pair Al–Y, with a local structure of comparatively strong bonding, involved in its amorphous structure as the basic structural element and the Ni being dispersed uniformly in the amorphous structure.

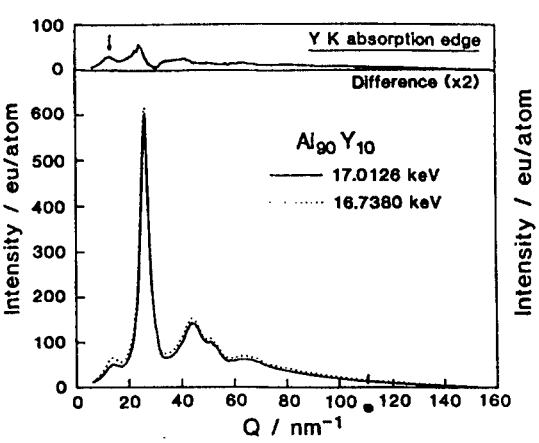

Figure 4. Environmental Structural Function of Amorphous Alloy $Al_{90}Y_{10}$ With Respect to Y

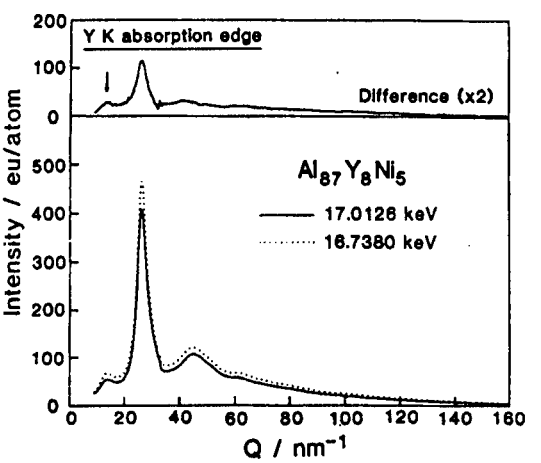

Figure 5. Environmental Structural Function of Amorphous Alloy $Al_{87}Y_8Ni_5$ With Respect to Y

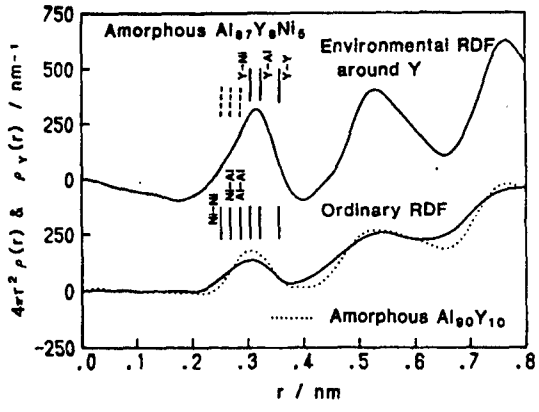

Figure 6. Radial Distribution Function and Environmental Radial Distribution Function for Amorphous Alloys $Al_{90}Y_{10}$ and $Al_{87}Y_8Ni_5$

Table 1. Atomic Correlations in the Closest Vicinity of an Atom in the Amorphous Alloys $Al_{90}Y_{10}$ and $Al_{87}Y_8Ni_5$

Amorphous $Al_{90}Y_{10}$				
Pairs	Ordinary RDF		Environmental RDF around Y	
	r/nm	N	r/nm	N
Al–Al	0.288	10.7±0.8		
Al–Y	0.320	1.6±0.2		
Y–Al	0.320	14.2±1.3	0.320	14.1±1.5
Y–Y	0.362	1.2±0.9	0.362	1.1±0.5
Amorphous $Al_{87}Y_8Ni_5$				
Al–Ni	0.268	6.5±0.2		
Ni–Al	0.268	0.4±0.1		
Al–Al	0.286	7.2±0.8		
Ni–Y	0.303	3.5±2.6		
Y–Ni	0.303	2.2±1.7	0.297	2.7±0.7
Al–Y	0.320	1.2±0.2		
Y–Al	0.320	13.5±2.7	0.320	14.3±1.9
Y–Y	0.356	0.8±0.6	0.356	0.4±0.4

The author expresses here his gratitude to Eichiro Matsubara and Masakazu Sugiyama for cooperation rendered in the execution of the research involved in the present report, and to the members of the staff, particularly Masaji Nomura, Tetsuya Ishikawa, and Atsushi Koyama, of the High Energy Physics Laboratory and the Synchrotron Radiation Experimental Facilities for the numerous helps extended in the experiment using synchrotron radiation.

References

1. Suryanarayana, C., "Rapidly Quenched Metals, Bibliography," IFI/Plenum Publication, New York, 1980.

2. Shechtman, D., Blech, I.A., Gratias, D., and Cahn, J.W., PHYS. REV. LETT., Vol 53, 1984, p 1951.

3. Inoue, A., Ohtera, K., Tsai, A.P., and Masumoto., T., JAPANESE J. APPL. PHYS., Vol 27, 1988, p L280.

4. For example, T.L. Hill, "Statistical Mechanics," McGraw-Hill, New York, 1956.

5. James, R.W., "The Optical Principles of the Diffraction of X-Rays," G. Bell & Sons, London, 1954.

6. For example, Y. Waseda, "Novel Application of Anomalous X-Ray Scattering for Structural Characterization of Disordered Materials," Springer-Verlag, Heidelberg, 1984.

7. Bancel, P.A., Heiney, P.A., Stephens, P.W., Goldman, A.I., Horn, P.M., PHYS. REV. LETT., Vol 54, 1985, p 2422.

8. Matsubara, E., Harada, K., Waseda, Y., Inoue, A., Bizen, Y., and Masumoto, T., J. MATER. SCI., Vol 23, 1988, p 3485.

9. Matsubara, E., Waseda, Y., Inoue, A., Ohtera, H., and Masumoto, T., ZEIT. FUR NATURFORSCH, Vol 44a, 1989, p 814.

Mechanical Properties of Amorphous Alloy Aluminum Series

906C7531F Tokyo AL KEI AMORUFASU GOKIN NO KOZO TO TOKUSEI in Japanese 6 Feb 90 pp 21-24

[Article by Yoshimasa Odera, Yoshida Kogyo, K.K.]

[Text] **1. Introduction**

Research on amorphous alloys, as started in the 1960s, led to development of those of the Fe, Co, and Ni series of the 1970s, which found practical applications in magnetic materials, among other things, because of their excellent properties[1]; research on the Al and Mg alloy series, which are representative of the light metal alloy series, was only slightly carried out. Researchers at Tohoku University, nevertheless, have recently discovered amorphous alloys of the Al series that have high strength and high corrosion resistance,[2-5] as well as those of the Mg series having high strength.[6] Of these, the present paper deals with mechanical properties, etc., of the Al series of amorphous alloys.

2. Two-Element Alloys of the Al-Ln Series (Ln: Rare Earth Element)

(1) Range of Formation of Amorphous Single Phase

Research on the liquid quench method was carried out on the two-element alloy series of Al-Si, Al-Ge, Al-Cu, Al-Ni, Al-Cr, and Al-Pd, with attempts to gain amorphous single phase from these alloys all failing, however. The two-element alloy series Al-Ca and Al-La, in turn, gave amorphous single phase, but exclusively in those that had high Ca and La content.

In 1987, the Al series of amorphous alloys that did not involve a submetal were prepared and, in the relevant series of experiments, the amorphous single phase was produced in Al-Ln series of two-element alloy even with compositions of high Al content.[7] Figure 1 presents the range of formation of amorphous single phase by means of the single roll method for the Al-Ln series of two-element alloy.[7] Also presented in the figure are compositions for relevant eutectic materials and intermetallic compounds except for the Al-Nd series. The Al-Sm series, meanwhile, forms amorphous single phase in the range of 84~92 at.% of Al, the widest of all the Al-Ln series.

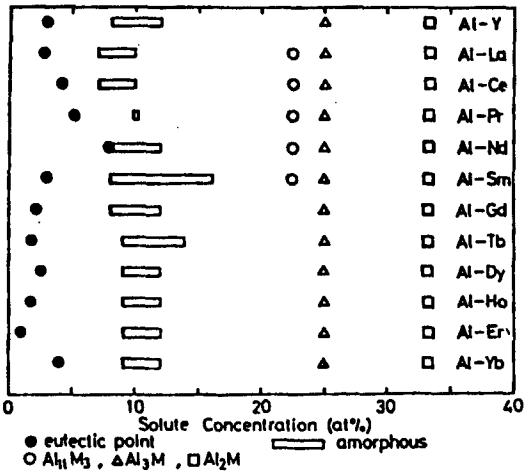

Figure 1. Domain for Formation of Amorphous Alloys for the Two-Element Alloys Al-Ni

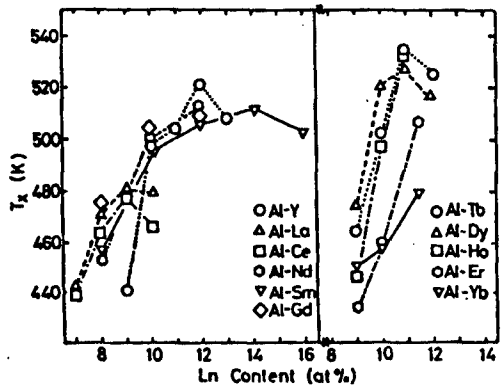

Figure 2. Dependence on Composition of Crystallization Temperature T_x for the Two-Element Alloys Al-Ln

(2) Thermal Stability of the Amorphous Phase

The relationship between crystallization temperatures T_x and the Ln content are presented in Figure 2. T_x initially rises rapidly with increasing amount of Ln, but turns approximately stationary after a certain value of Ln content is reached. In compositions in which T_x rises rapidly, Al is first crystallized out as the temperature is raised out and then the relevant metallic compounds are at higher temperatures. In compositions where T_x stations stationary, in contrast, the intermetallic compounds crystallize out from the beginning. The maximum T_x values for these alloy series range from 480 K to 537 K, but no orderly relationship between T_x and the atomic numbers of these series of alloys are notable.

(3) Mechanical Properties

Figure 3 presents the relationship between the Vickers hardness and the amount of Ln for two-element alloys of the Al-Ln series. The hardness is above 210 for all of the Al-Ln series and, in particular, as high as 270 for the alloy $Al_{88}Dy_{12}$. This amorphous alloy series may be subjected to bending through an angle of 180° to allow intimate contact of the bent two halves and exhibits a sticky property. In addition, the Al-Y, Al-La, Al-Ce, Al-Sm, Al-Dy, and Al-Tb series of this Al-Ln alloy series, displays tensile strengths as high as 700 MPa and above.

3. Three-Element Alloys of Al-Ln-TM Series (TM: Transition Metal)

Three-element alloys of the Al-Ln series proved to be amorphous single phase on the Al-rich side, which was of higher strength than conventional Al alloys. Ce, which displayed high strength as an Ln among the Al-Ln series of two-element alloys and was the cheapest of all the Lns, was selected and, to this Al-Ce series, was added the transition element Cr, Mn, Co, Ni, Cu, or Nb as

the third element to form an amorphous single phase, of which the range of formation is presented in Figure 4. This range gradually expands with increasing atomic number and reaches the maximum value at Ni, and then gradually narrows—a tendency that is also seen in cases where other rare-earth elements are chosen as the alloy component.

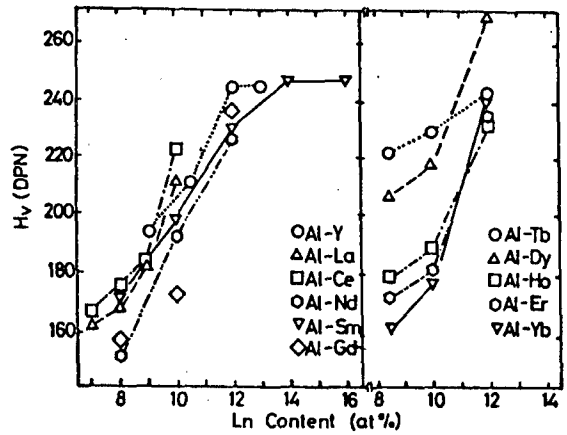

Figure 3. Dependence on Composition of Vickers Hardness for the Two-Element Alloys Al-Ln

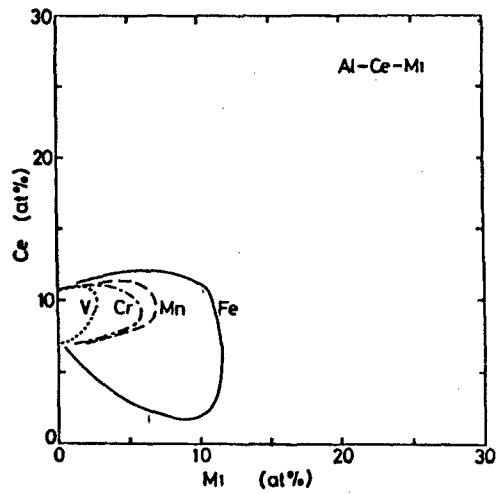

Figure 4. (a) Domain for the Formation of Amorphous Alloys for the Three-Element Alloy Al-Ce-M_1 (M_1: V, Cr, Mn, Fe)

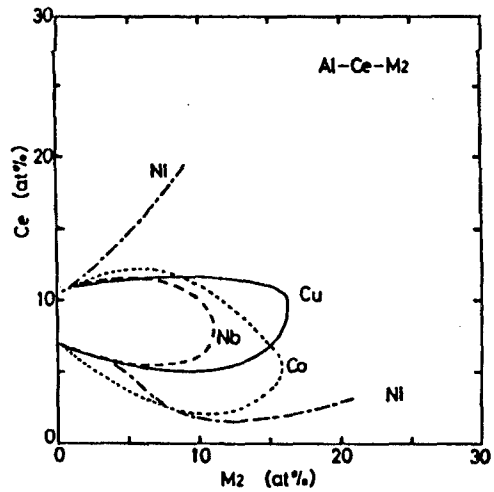

(b) Domain for the Formation of Amorphous Alloys for the Three-Element Alloy Al-Ce-M_2 (M_2: Co, Ni, Cu, Nb)

(2) Thermal Stability of the Amorphous Alloy

The relationship between T_x and the relevant composition, as representing the thermal stability of the Al-Ce-TM alloy series of three-element alloy, is presented in Figure 5. The figure shows a plot of T_x vs. the amount of TM, with the amount of Ce fixed at 15 at.%. T_x rises with anincreasing amount of Mn, Fe, Co, or Nb and, in the case of $Al_{60}Ce_{10}Ni_{30}$, reaches as high as 734 K.

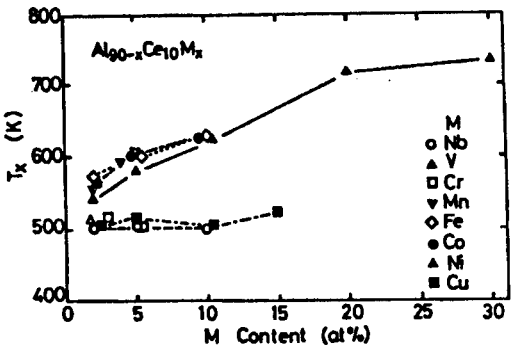

Figure 5. Dependence on Composition of Crystallization Temperature T_x for the Three-Element Alloy Al-Ce-M (M: Nb, V, Cr, Mn, Fe, Co, Ni, Cu)

Where the metals Cr, Cu, and Ni are concerned, T_x is nearly stationary at around 500 K. In cases where a TM is fixed at 10 at.% and the amount of Ce is varied, T_x rises with increasing amount of Ce and, in the case of Ni being involved as the TM, in particular, T_x rises by about 200 K or more as the amount of Ce is varied from 2~10 at.%.

(3) Mechanical Properties

Table 1 presents results of measurements on the Al series of amorphous alloy for tensile strength, Young's modulus, elongation, and Vickers hardness. Whereas the three-element alloy of the Al-TM submetal series $Al_{75}Ni_{10}Si_{15}$ has a low 440 MPa for tensile strength,[8] that of the Al-Ln-TM series exhibits as high a strength as 1,140 MPa maximally.[4,9] Of the three-element alloy of the Al-Ln-TM series, some series of the alloy exhibit glass transition behavior; the dependence on temperature of tensile strength, Young's modulus, and elongation, for one of these alloys, the amorphous alloy $Al_{85}Y_{10}Ni_5$, is presented in Figure 6. The tensile strength falls gradually as the temperature rises, but a strength as high as about 700 MPa is retained at 450 K. The Young's modulus, in turn, falls gradually with rising temperature and then rapidly at temperatures above that of glass transition, reaching, at temperatures just below the T_x, down to 30 percent of its level at room temperature. The elongation, finally, rises as the temperature exceeds that of glass transition and reaches about 8 percent at temperatures just below that of T_x. It is possible to obtain solid amorphous moldings by utilizing this characteristic glass transition behavior.

4. Mechanical Properties of Molded Bulky Specimens

Various properties of the alloy specimens in ribbon form, 30 μm in thickness and 1 mm in width, produced by the single roll method was described above: those of an alloy specimen prepared by solidifying and molding the alloy powder follows.

The alloy powder for moldings was an amorphous powder produced with a superhigh pressure gas-atomization apparatus, and solidified and molded by hot pressing or warm extrusion. Because alloy moldings prepared by hot pressing

are limited in size, although it allows comparatively ready formation of the moldings, the warm extrusion has been the author's method of choice for the moldings of amorphous alloys. Extruded specimens exhibit a slightly lower strength than those in ribbon form because of the effects of oxides involved, among other things.

Table 1. Mechanical Properties of Representative Amorphous Alloys of the Al Series

Alloy	σ_f (MPa)	E (GPa)	ϵ (%)	H_V
$Al_{75}Si_{15}Ni_{10}$	440	—	1.4	370
$Al_{85}Zr_5Ni_{10}$	800	80.4	1,0	340
$Al_{87}Y_8Ni_5$	1,140	71.2	1.6	300
$Al_{85}Y_{10}Ni_5$	920	62.8	1.5	320
$Al_{84}La_6Ni_{10}$	1,010	83.6	1.2	285
$Al_{84}Ce_4Mg_2Ni_{10}$	1,100	68.7	1.6	340
$Al_{84}Ce_4La_2Ni_{10}$	980	75.4	1.3	320
$Al_{90}Ce_5Fe_5$	940	66.0	—	—
$Al_{87}Gd_{4.3}Fe_{8.7}$	840	53.0	—	—
$Al_{87}Y_{4.3}Ni_{8.7}$	880	50.0	—	—

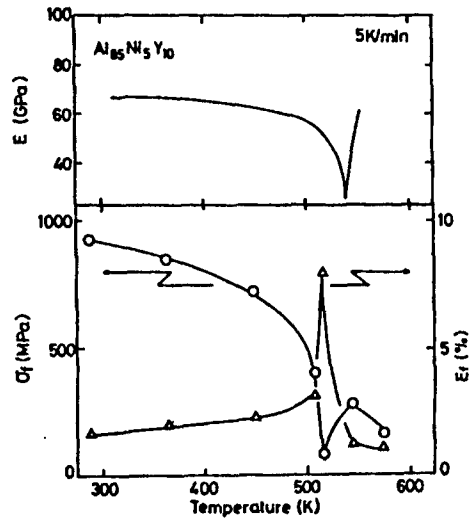

Figure 6. Dependence on Temperature of the Tensile Strength, Young's Modulus, and Elongation of the Amorphous Alloy $Al_{85}Ni_5Y_{10}$

An experiment running parallel with the above has been aimed at preparation of crystalline specimens from the identical amorphous alloy powder by extrusion, with the temperature for extrusion raised to a level higher than that of crystallization. The tensile strength of the resulting specimen has proved to be approximately equal to that of the ribbon-form specimen, but the value of Young's modulus larger by 40~50 percent.

5. Conclusion

The Al series of amorphous alloy has been dealt with above. The relevant research has currently been centered on the solidification and molding of the powder, but perfect molded material has yet to be made available because of lack of adequate temperature control in the relevant process. The desired material, therefore, may be made available by improving this poor temperature control. In connection with corrosion resistance, the other feature of Al, amorphous alloys of the Al series having high corrosion resistance have also been developed, although the above discussion has largely been centered on their mechanical properties.

References

1. Masumoto, T. (compiling and writing), "Basis of Amorphous Metals," Ohm Co., Ltd., 1982.

2. Tsai, A.P., Inoue, A., Masumoto, T., MET. TRANS., Vol 19A, 1988, p 391.

3. Inoue, A., Ohtera, K., Thai, A.P., and Masumoto, T., JPN. J. APPL. PHYS., Vol 27, 1988, p L479.

4. Ibid., p L280.

5. Ibid., Int. Meeting on Advanced Materials, Materials Research Society, Tokyo, May 1988, in press.

6. Inoue, A., Ohtera, K., Kita, K., and Masumoto, T., JPN. J. APPL. PHYS., Vol 27, 1988, p L2248.

7. Inoue, A., Zhang, T., Kita, K., and Masumoto., T., MATER. TRANS. JAPAN INST. METALS, in press.

8. Inoue, A., Yamamoto, M., Kimura, H.M., and Masumoto, T., J. MATER. SCI. LETT., Vol 6, 1987, p 194.

9. He, Y., Poon, S.J., and Shiflet, G.J., SCIENCE, Vol 23, 1988, p 1640.

Electronic Properties of Amorphous Al Series Material

906C7531G Tokyo AL KEI AMORUFASU GOKIN NO KOZO TO TOKUSEI in Japanese 6 Feb 90 pp 25-28

[Article by Uichiro Mizutani, Engineering Department, Nagoya University]

[Text] 1. Introduction

Inoue, et al., reported in 1987 a method for preparing Al-based amorphous alloys, using the liquid quenching method, by adding 10~30 at.% of a transition metal to Al-Si or Al-Ge.[1] The unique structure and characteristic physical properties of the product were also reported, one intriguing item being that it has resistivity as high as 1,000 $\mu\Omega$-cm despite high Al contents. The author, et al., have been systematically discussing the mechanism of electric conductance of diamagnetic amorphous alloys on the basis of their electronic structure.[2] In the Al-based amorphous alloys developed by Inoue, et al., Ni seems to involve minimum magnetic effect on the electronic properties as a transition metal to be coupled with Al. Al-Ni-Si and Al-Ni-Ge series, indeed, are diamagnetic, which coupled with their Al rich composition allows sp-electrons to dictate the electric conduction.[3] These series thus represent basic ones for research on electric conduction of the irregular series. The author, et al., also directed their attention to the three-element series Al-Ni-X, where X denotes Ti, Zr, or La.[4] Where the Al content is nil, Ni-Zr and Ni-Ti make typical amorphous alloys of the d-electron series. If Al is added to these d-electron series, and a continuous series of amorphous alloys with increasing content of Al up to the Al-rich region are prepared, it may be possible to examine how the electronic properties of the alloys vary as the relevant electronic structures change from the d-electron system to the sp-electron one and, thus, important information for the role of the d-electron in different physical properties may conceivably be made available. Al-Li-Cu, Al-Ru-Cu, and other quasicrystals, in turn, have been spotlighted recently. It is also Al here that plays the leading role. These series also represent the sp-electron series and are important in studying the effect of the quasi-crystal structure on the conducting electrons.[5,6] It is particularly intriguing to study the relationship between the sp-electron series of amorphous alloys and their physical properties. The author discusses below the Al series of amorphous alloy and the physical properties of quasicrystals.

2. Electronic Structure of the Al Series of Amorphous Alloy

The amorphous alloys $Al_{100-y-x}Ni_ySi_x$ (where $10\leq x\leq 35$, $10\leq y\leq 20$), $Al_{100-y-x}Ni_{10}Ge_x$ (where $10\leq x\leq 35$), and $(Ni_{67}X_{33})_{1-x}Al_x$ (where X=Ti, Zr, or La and $0\leq x\leq 0.85$) were prepared by the liquid quenching method,[3,4] but $(Ni_{67}Zr_{33})_{0.5}Al_{0.5}$ and $(Ni_{67}Ti_{33})_{0.5}Al_{0.5}$ of these were prepared by the sputtering method. Figure 1 presents patterns of the valence electron zone produced by X-ray photoelectron photoscopy (XPS) for $Al_{90-x}Ni_{10}Si_x$ (where $15\leq x\leq 35$). The peak, centered at a bonding energy of about 3 eV, represents the Ni-3d band and, as it declines toward the Fermi level, shows a distinct nicking at around 2 eV where the Ni-3d band terminates and the sp band starts to govern down to the Fermi level, that is, this series belongs to the sp series. Where the alloy series $(Ni_{67}Zr_{33})_{1-x}Al_x$ were evaluated in the same manner, the result proved that the Fermi level was dictated by Zr-4d for x=0~50, but that a distinct nicking was notable at the lower-bonding-energy end of the d-band, just as it was in Figure 1, for $x\geq 0.65$, indicating that the Fermi level was under the sp bond control. This implies that this alloy series represents d-electron series where $x\leq 0.6$, but sp-electron series where $x\geq 0.65$. This change in band structure was also reflected in the coefficient of electronic specific heat, as seen in Figure 2. The plot showed that the alloy series $(Ni_{67}Zr_{33})_{1-x}Al_x$ turned into the sp series as the Al content x exceeded 0.65, that all Al-Ni-Si and Al-Ni-Ge series were sp series, and that, in the latter two series in particular, the density of state at the Fermi level fell rapidly as the contents of Si or Ge rose, that is, Al content fell below 0.65.

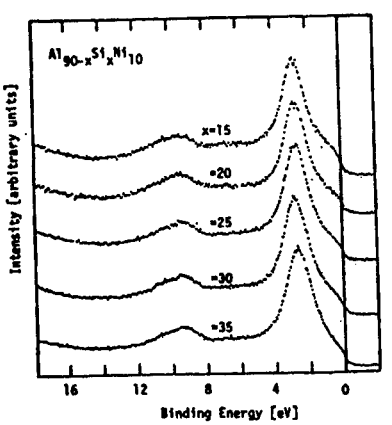

Figure 1. XPS of Valence Band Electrons for Amorphous Alloy Al-Ni-Si
(The origin is the Fermi level.[4])

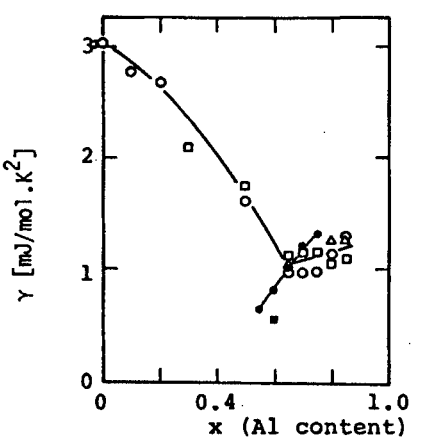

Figure 2. Electronic Specific Heat Coefficient for the Alloys[4]
o: Al-Ni-Zr; □: Al-Ni-Ti;
Δ: Al-Ni-La; •: Al-Ni-Si;
■: Al-Ni-Ge

3. Electrical Resistance of the Al Series of Amorphous Alloy

Figure 3 represents a plot of resistivity vs. Al content at 300 K. Whereas the resistivity of $(Ni_{67}X_{33}X_{1-x}Al_x$ exhibited a gradually rising and falling peak centered at approximately x=0.5, those of Al-Ni-Si and Al-Ni-Ge displayed

rapidly rising peaks in the range $x \leq 0.65$. It was notable that the resistivity of the former series, as they turned into d-electron series, did not undergo rapid changes but fell gradually toward the value at $(Ni_{67}Zr_{33})_1Al_0$. That resistivity falls with the rising number of d-electrons may conceivably provide evidence for the major contribution of d-electrons in enhancing electric conduction. The relationship between resistivity and electronic specific heat for the above alloys, together with those for other series of amorphous alloys so far evaluated, are summarized in Figure 4. The relationship between resistivity ρ and the coefficient of electronic specific heat γ or the density of state at the Fermi level N(EF) is given by

$$\rho^{-1} = \left(\frac{\pi^2}{3}\right) \Lambda_F V_F N(EF) \tag{1}$$

If one assumes here that the mean free path of the electron Δ_F and Fermi velocity F_F take the least possible value in the high resistivity region and, hence, constant values, ρ and γ then must exhibit a reciprocal relationship, as shown by the dotted line in the figure; data for the d-electron system falls under the line. That the fall in value of γ and, hence, that of the number of d-electrons, never fails to lead to an increase of ρ indicates that d-electrons contribute to conduction in a large measure. The sp-electron series, in turn, concentrate their data in the low γ region, and it can be seen from the figure that a decrease in γ causes a steep rise in ρ. Not only does a decrease in the number of electrons lead to an increase in ρ, but a decrease in the value of mean free path underlies this, as shown by dependence of electric resistance on temperature.

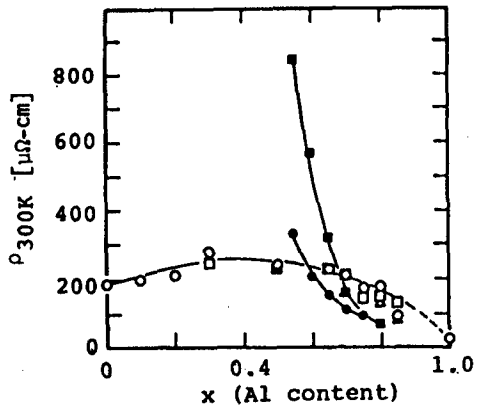

Figure 3. Resistivity for the Alloys[4]
o: Al-Ni-Zr; □: Al-Ni-Ti;
Δ: Al-Ni-La; •: Al-Ni-Si;
■: Al-Ni-Ge

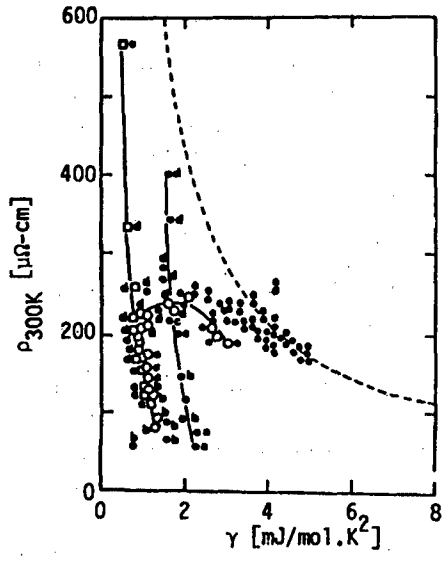

Figure 4. Relationship Between ρ and γ for the Alloys[4]
□: Al-Ni-Si (or Ge);
o: Al-Ni-X (X=Zr, Ti, La)

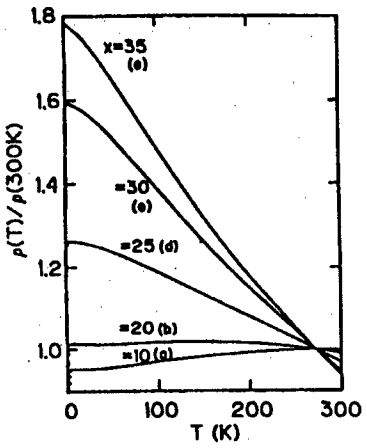

Figure 5. Dependence on Temperature of the Resistance of the Amorphous Alloy $Al_{90-x}Ni_{10}Ge_x$[4]

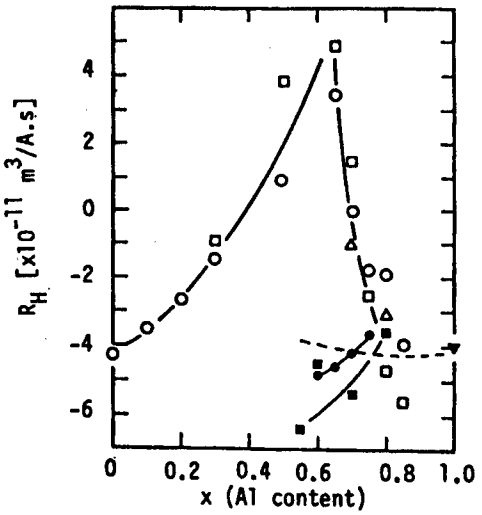

Figure 6. Hall Coefficient for the Alloys[4]
o: Al-Ni-Zr; □: Al-Ni-Ti;
Δ: Al-Ni-La; •: Al-Ni-Si;
■: Al-Ni-Ge

The ρ-T characteristics of all diamagnetic amorphous alloys may be grouped into five types.[2,4] Figure 5 presents ρ-T curves for the Al-Ni-Ge series. With increasing resistivity, the type changes (a)→(b)→(c)→(d)→(e) in that order. The changes (a)→(b)→(c) are well interpretable by the generalized Faber-Zeeman theory based on the Boltzmann transport equation. Here the process of shortening the mean free path is of more importance than changes in relevant electronic state.2,4 The types (d) and (e) are not interpretable by the above classical scattering mechanism, however. They appear in the high resistivity region, where the mean free path shortens and approaches the level of mean atomic distance, namely, in the vicinity of the dotted line in Figure 4. Of the sp-electron series, the type-(e) curve is found in the Al-Ni-Ge series in cases where ρ exceeds 500 $\mu\Omega$, among other things, whereas the d-electron series is always present as type (e). In Figure 4, type of ρ-T curve for each of the curves is entered. It can be seen from the figure that the Al-Ni-Si and Al-Ni-Ge series are typical sp series, whereas the $(Ni_{67}Zr_{33})_{1-x}Al_x$ series changes from the sp-electron series to the d-electron series.

4. Hall Coefficient for Al Series of Amorphous Alloy

Figure 6 presents dependence on Al concentration of the Hall coefficient for the Al-Ni-Si and Al-Ni-Ge series and for the $(Ni_{67}X_{33})_{1-x}Al_x$ series, where X denotes Ti, Zr, or La. In the former two series, which are sp-electron series, the coefficient increases in absolute value in the negative direction with increasing content of Si or Ge, which implies a fall in the number of the carriers, and runs parallel to the fall of the electronic specific heat coefficient and the rise of resistivity. In the latter series, in turn, the Hall coefficient is converted to positive values as the electronic state is turned from the sp- to d-electron series. A positive Hall coefficient is characteristically observed in the d-electron series.[7]

5. Crystallization Temperature of Al Series of Amorphous Alloy

On the basis of Lindemann's fusion formula, the melting point T_m is related to Debye temperature γ_D by the formula

$$x_m = \left(\frac{3\hbar}{\theta_D}\right)\left(\frac{T_m}{MK_B}\right)^{1/2}\left(\frac{4\pi}{3V}\right)^{1/3} \tag{2}$$

where x_m denotes the root-mean-square (rms) of the displacement of an atom, as standardized by the average radius of the atom; M the average mass of the atom; and V the volume per atom. Since melting is equivalent to crystallization in amorphous alloys, the melting point T_m in formula (2) may be replaced by the crystallization temperature T_x in the discussion. A replacement of the value of T_m by that of T_x, indeed, affords a value of x_m of around 0.2, irrespective of the kind of the alloy and, with x_m at such a constant value, a correlation between the crystallization temperature and Debye temperature seems to be possible. Figure 7 presents the relationship between T_x and θ_D for diamagnetic amorphous alloys measured to date. It is seen that the d-electron series and sp-ones are clearly divided; that is, the d-electron series has a higher crystallization temperature than the sp-ones for the same Debye temperature. Where $(Ni_{67}X_{33})_{1-x}Al_x$ (X=Ti, Zr, or La) is concerned, at 0.65 as the dividing point, one is on the top line and the other on the bottom. These demonstrate that the crystallization temperature largely reflects the binding energy of electronic structure of relevant atoms.

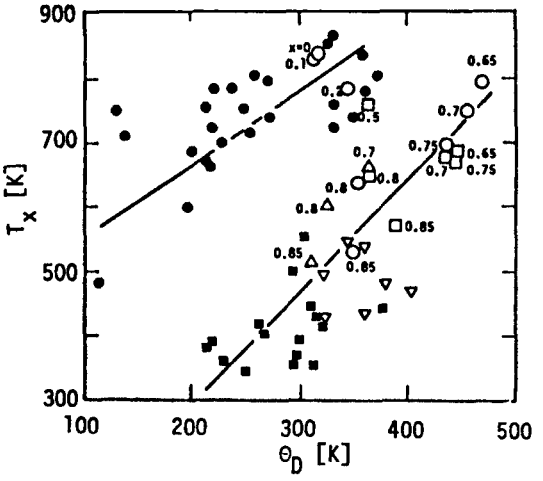

Figure 7. Relationships Between T_x and θ_D for the Nonmagnetic Alloys (Numerical value attached is the Al concentration x.)[4]
v: Al-Ni-Si (or Ge); o□Δ: Al-Ni-X (X-Zr, Ti, La)

6. Electronic Structure of the Quasicrystals of the sp-Electron Series

Figure 8 presents the dependence on the average valence electron number $(e/a)_n$ of the electronic specific heat coefficient γ for various sp-electron series of quasicrystals. As opposed to amorphous alloys, the γ value tends to fall rapidly as the $(e/a)_n$ value falls and approaches 2. The Brillouin zone effect

is also stronger, conceivably reflecting the density of state—which is intriguing in view of divalent metals having essentially an electronic structure for insulation materials. It was also found that the quasicrystals Al-Li-Cu[5] and Al-Ru-Cu[8] had extremely small electronic specific heats in comparison with their relevant free electron values,[8] but that they had resistivity as large as 1,000 $\mu\Omega$-cm. In quasicrystals where the Bloch wave is not stable, unlike that of crystal, the small number of carriers involved may have led directly to an increase of resistivity. Relevant data, as seen in Figure 4, showed up in the vicinity of the dotted line in the region where γ is small.

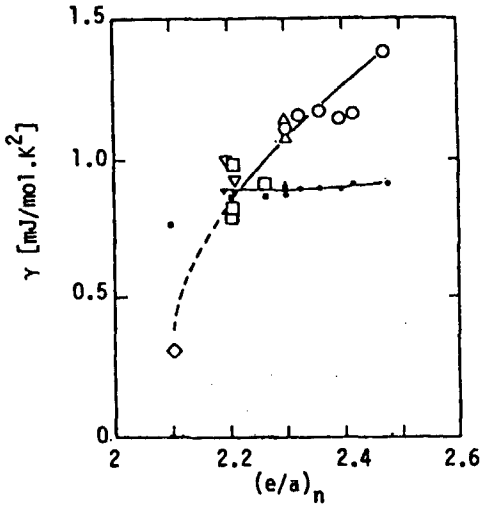

Figure 8. Electronic Specific Heat of the Quasicrystals of the sp-Electron Series for the Alloys.
(Corresponding black marks are those for free electrons.[6])
o: Al-Cu-Mg; Δ: Al-Ag-Mg; □: Mg-Ga-Zn; ▽: Al-Zn-Mg;
◇: Al-Li-Cu

The ρ-T characteristics of quasicrystal of the sp-electron series are similar to those for the amorphous alloy of the same series.[5-6] It was pointed out that resistivity increased as the quasicrystal quality was improved by heat treatments[6]—an interesting result that is not interpretable by the generalized Faber-Zeeman theories. Crystal grains of the quasicrystal Mg-Zn-Ga produced by the liquid quench measure only about 100 Å even after thermal treatment.9 The resistivity of single quasicrystals of the sp-electron series, as unaffected by the grain boundary effects, may be extremely large, and such quasicrystals, which are close to perfection, may conceivably exhibit a ρ-T characteristics entirely different from those of amorphous alloys; indeed, dependence on temperature of thermoelectric power and Hall coefficient proved to be characteristically different from those of amorphous alloys.[6]

The author finally adds that the research on Al-based amorphous alloys was made jointly with Kazuhide Tanaka of Nagoya University, Kazuaki Fukamichi of Tohoku University, and Takeshi Matsuda of Aichi Educational University, and the research on Al-based quasicrystals was with Shin Takeuchi, and Kaoru Kimura, both of Tokyo University, and Takeshi Matsuda of Aichi Educational University.

References

1. Inoue, A., Yamamoto, M., Kimura, H.M., and Masumoto, T., J. MAT. SCI. LETTERS, Vol 6, 1987, p 194.

2. Mizutani, U., MAT. SCI. ENG., Vol 99, 1988, p 165; SUPPL. TO TRANS. JIM, Vol 29, 1988, p 275.

3. Yamanaka, E., Yamada, Y., Ohara, I., Matsuda, T., and Mizutani, U., SUPPL. TO TRANS. JIM, Vol 29, 1988, p 329.

4. Mizutani, U., Ohashi, S., Matsuda, T., Fukamichi, K., and Tanaka, K., to appear in J. PHYS.: CONDENSED MATTER, 1989.

5. Kimura, K., Iwahashi, H., Hashimoto, T., Takeuchi, S., Mizutani, U., Ohashi, S., Ito, G., J. PHYS. SOC. JPN., Vol 58, 1989, p 2472.

6. Mizutani, U., Sakabe, Y., and Matsuda, T., submitted to J. PHYS.: CONDENSED MATTER, 1989.

7. Manh, D. Nguyen, Mayou, D., Cyrot-Lackmann, F., and Pasturel, A., J. PHYS. F.; MET. PHYS., Vol 17, 1987, p 1309.

8. Mizutani, U., Kimura, K., Takeuchi, S., to be published.

9. Tanaka, N., private communications.

Hydrogen Absorption by Amorphous Al-Series Alloy, Relevant Mechanical Alloying

906C7531H Tokyo AL KEI AMORUFASU GOKIN NO KOZO TO TOKUSEI in Japanese 6 Feb 90 pp 29-30

[Article by Kenji Suzuki, Research Institute for Iron, Steel, and Other Metals, Tohoku University]

[Text] **1. Introduction**

Amorphous alloys constituted largely by a transition metal or a rare earth metal are produced with ease from relevant liquids by super rapid quench solidification. On contrast, preparation of an amorphous alloy from the liquid of a light metal alloy of the Al or Mg series by that method generally involves substantial difficulty. In addition, the amorphous alloys of the light metal series are pronouncedly lower in stability than those of the transition metal or rare earth group. It has been shown recently, however, that the Al-based three-element series of amorphous alloy involving one of some transition metals or of some rare-earth-group metals display an extremely extended region of supercooled liquid.

The author, et al., have been conducting neutron-scattering and X-ray diffraction experiments with the view to examining the capacity of the Al and Mg series of alloy for forming an amorphous alloy and to determining the cause of the lack of stability of the alloy in terms of their atomic structures. In particular, noting the possibility of application of the Al series of amorphous alloy in hydrogen storage alloy, Y and La of high hydrogen-storage capacity have been selected as an alloy element. The present lecture is concerned with the short range structure of the Mg-Zn series of amorphous alloy, the physical properties of which are comparatively well known, as representing the light metal alloy; the position of the stored hydrogen atoms of the Al-Y series of amorphous alloy; and mechanical alloying of the Al-Ta series of amorphous alloy.

2. Short-Range Structure of the Mg-Zn Series of Amorphous Alloy

X-ray diffraction measurements were carried out on the three different kinds of amorphous alloy Mg_xZn_{100-x}, where x were 65, 70, and 75, and which had been prepared by super rapid quench solidification of the relevant material in the

liquid state under an Ar atmosphere using the single roll method. Assuming that the dependence of composition of the partial structure of the amorphous alloy of Mg–Zn series might be ignored in this narrow range of compositions, the relationships of Mg–Mg, Mg–Zn, and Zn–Zn were estimated separately, as shown in Figures 1 and 2 and in Table 1. The features of the amorphous alloys of Mg–Zn series, as opposed to those for transition metal series, may be summarized as follows:

(a) The prepeak at $Q \simeq 1.5$ A^{-1} in the plot of the structural factors S(Q) vs. the wave vector Q in Figure 1 involves not only a contribution from the same element species Zn–Zn, but also one from the different element species Zn–Mg.

(b) The short range structure of the Mg–Zn series of amorphous alloy is much less orderly than that of the corresponding crystal $Mg_{51}Zn_{20}$; the constituent elements are rather close to chaos.

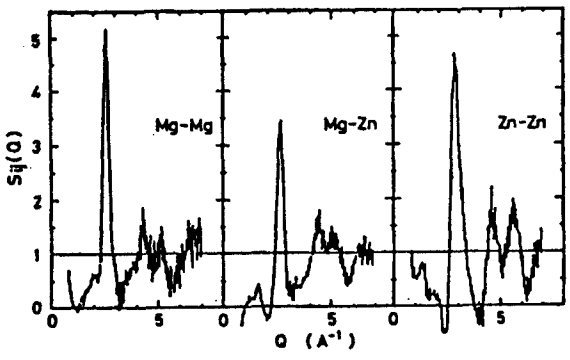

Figure 1. Partial Structural Factor of the Amorphous Alloy $Mg_{70}Zn_{30}$

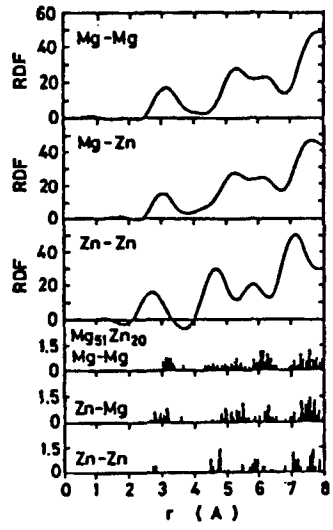

Figure 2. Partial Radial Distribution Function for the Amorphous Alloy $Mg_{70}Zn_{30}$ and for the Crystal $Mg_{51}Zn_{20}$

It has been revealed, in contrast, that the transition metal series of amorphous alloy have a chemical short-range structure wherein that of corresponding crystals is well retained.

The thermal effect of the position of the main peak for S(Q) or g(r) in the Mg–Zn series of amorphous alloy, in turn, is quantitatively related to the macroscopic thermal expansion, as seen in Figure 3; the height of the peak, however, apparently rises with increasing temperature, as seen in Figures 4 and 5, which may be taken as a kind of "motional narrowing." Hafner, in 1982, predicted on the basis of a computer simulation that the g(r) peak grew unsymmetrically broad with increasing density.

Table 1. Interatomic Distances and Number of Coordinations for Three Correlations of the Amorphous Alloy $Mg_{70}Zn_{30}$ and the Crystal $Mg_{51}Zn_{20}$

	Amorphous $Mg_{70}Zn_{30}$		Crystal $Mg_{51}Zn_{20}$	
	r(A)	n(atoms)	r(a)	n(atoms)
Mg–Mg	3.15	10.5	3.198	9.43
Zn–Mg	3.05	7.5	3.004	9.95
Zn–Zn	2.68	3.7	2.764	2.00
Total		12.8		12.94

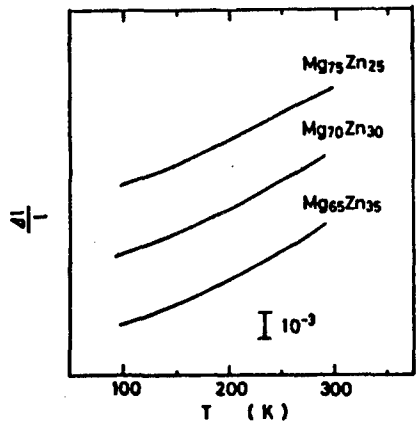

Figure 3. Thermal Expansion for the Mg–Zn Series of Amorphous Alloy

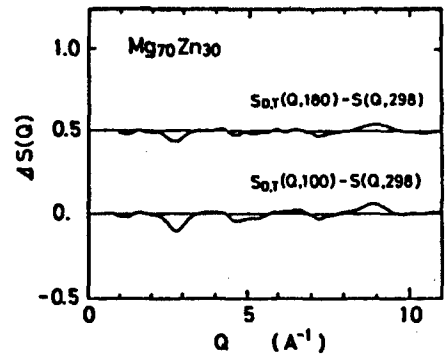

Figure 4. Dependence on Temperature of the X-Ray Structural Factor for the Amorphous Alloy $Mg_{70}Zn_{30}$

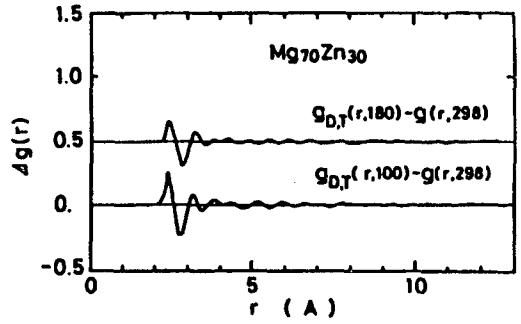

Figure 5. Dependence on Temperature of the X-Ray Two-Element Correlation Function for the Amorphous Alloy $Mg_{70}Zn_{30}$

3. Hydrogen Storage of the Al-Y Series of Amorphous Alloy

Alloys of Al_xY_{1-x} are turned into the amorphous state in the range x = 0.25~0.5 by the single roll liquid rapid quench solidification method. The temperature of crystallization for the Al–Y series of amorphous alloy ranges from

600~800 K, a level somewhat lower than that for the transition series. The crystallization is composed of multiple stages and is complex.

Figures 6 and 7 present the neutron total-structural factor S(Q) and total radial distribution factor (RDF) for the amorphous alloy $Al_{0.5}Y_{0.5}D_x$. The deuterium D_2 was absorbed into ribbons of the amorphous alloy $Al_{0.5}Y_{0.5}$ at 220°C and at 20 atm under the D_2 atmosphere. Features of the $Al_{0.5}Y_{0.5}$ series of amorphous alloy having absorbed hydrogen, which are notably different from those for the transition metal series, may be summarized as follows:

(1) An intensive small angle scattering is notable in the low scattering vector region ($Q \leq 1$ Å^{-1}) of the neutron S(Q), whereas no small angle scattering is seen in the X-ray S(Q). It is concluded from this that a fluctuation of average length around 7~10 Å takes place in the D_2 atom distribution; the transition metal series of amorphous alloy having absorbed hydrogen, however, seldom cause such a fluctuation in hydrogen atom distribution.

(2) The peak present at r = 2.3 Å in the RDF of amorphous alloy $Al_{0.5}Y_{0.5}$ in Figure 7 indicates that the D-Y bonding takes place in favor over the other ones in the process of absorption of D into the amorphous alloy. In particular, the atoms closely surrounding the atom are exclusively those of Y, with those of Al excluded. With increasing content of D atoms, the local arrangement of Y atoms just around the D atoms varies continuously from six-fold octahedron to four-fold tetrahedron, as can be seen in Figure 8. In cases where a D atom occupies the center of a six-fold octahedron, in particular, this series of alloy scarcely expands in volume but, rather, suffers shrinkage, as concluded from data of the relevant density measured.

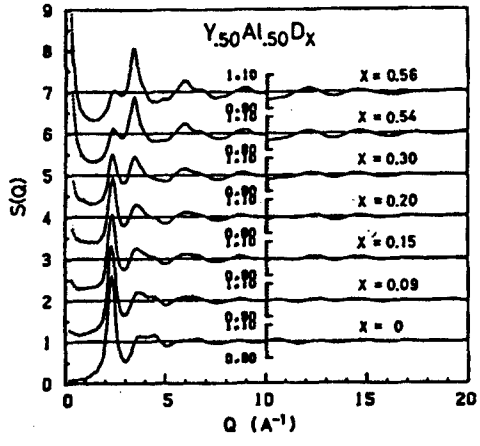

Figure 6. Neutron Total Structural Factor for the Amorphous Alloy $Al_{0.5}Y_{0.5}D_x$

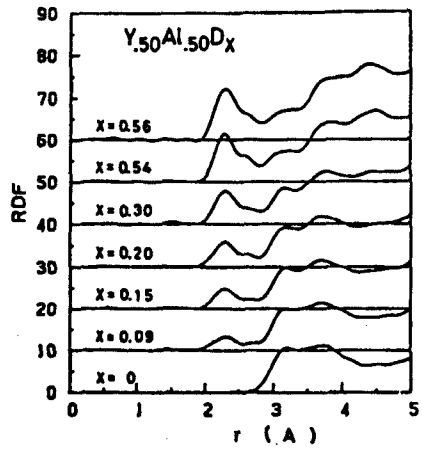

Figure 7. Neutron Total Radial Distribution Function for the Amorphous Alloy $Al_{0.5}Y_{0.5}D_x$

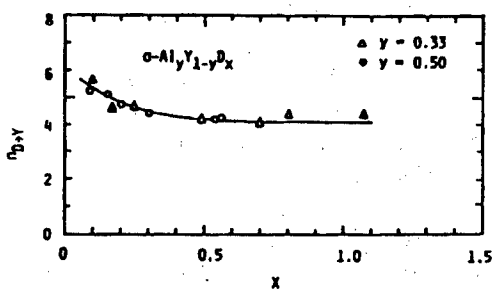

Figure 8. Number of Coordination of D Atoms Around a Y Atom

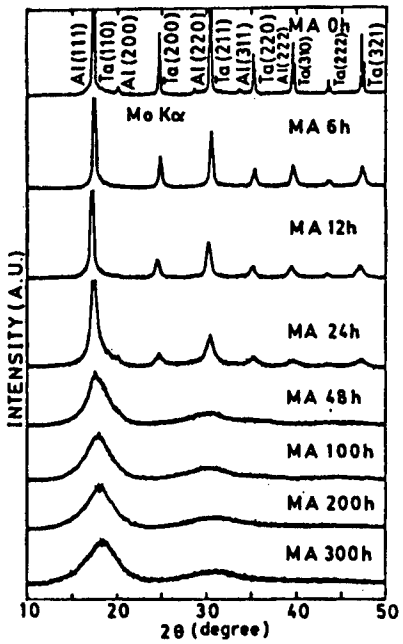

Figure 9. Changes in X-Ray Diffraction Pattern of a Mixture of Al and Ta Crystalline Powders by Mechanical Alloying Process

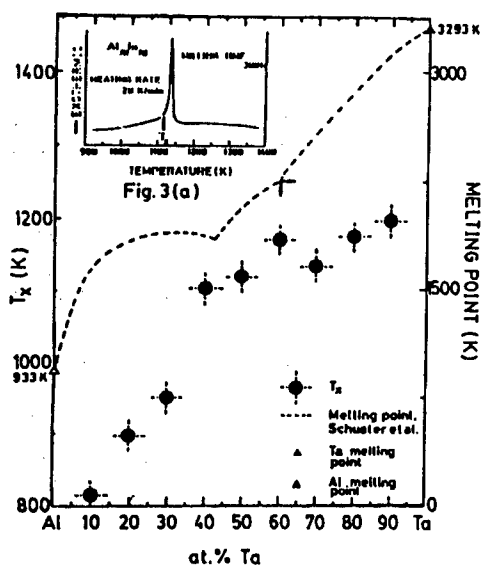

Figure 10. Temperature of Crystallization for the Al-Ta Series of Amorphous Alloy

4. Preparation of the Al-Ti Series of Amorphous Alloy by Mechanical Alloying

With a notable difference between the melting points of Al and Ta of 933 K and 3,293 K, respectively, it is not easy to produce an amorphous alloy of Al-Ta series by the common liquid rapid-cooling method. Nevertheless, the author was able to prepare it readily by subjecting the starting material crystals of Al(fcc) and Ta(bcc) to mechanical alloying under an Ar atmosphere.

Figure 9 presents the process of formation of the amorphous alloy $Al_{30}Ta_{70}$ by mechanical alloying as an example. It is concluded from this X-ray diffraction experiment that the direct reaction for the formation of the alloy of Al(fcc) + Ta(bcc) → Al_xTa_{1-x} proceeds with no intermediate product intervening; the formation of the amorphous alloy tends to accelerate in the period between the 24th to 48th hours of milling; the crystallization temperature for this alloy reaches as high as 1,200°C on the Ta-rich side; the dependence on the alloy composition of the crystallization temperature is presented in Figure 10.

Acknowledgement

The author expresses here his deep gratitude to the aid rendered by the Light Metal Foundation to the present research, which was conducted jointly with Toshiharu Fukunaga, Noriyuki Hayashi, and Mohamed Sherif El-Eskandarany.

References

1. Fukunaga, T., Sugawara, T., Itoh, F., and Suzuki, K., "Partial Structure Separation and Temperature Dependence of X-Ray Total Structure for Mg-Zn Amorphous Alloys," Z. PHYS. CHEM. NEU FOLGE, Vol 157, 1988, p 79.

2. Suzuki, K., "Atomic Scale Structure of Hydrogenated Amorphous Alloys by Pulsed Neutron Scattering," KEY ENGINEERING MATERIALS, Vol 13/15, 1987, p 697.

3. El-Eskandarany, M.S., Itoh, F., Aoki, K., and Suzuki, K., "Preparation of Al_xTa_{1-x} Amorphous Alloy Powders by Mechanical Alloying," PROC. LAM-7, 1989.

Transformation Into Amorphous State of Intermetallic Compounds in Aluminum by Mechanical Alloying

906C7531I Tokyo AL KEI AMORUFASU GOKIN NO KOZO TO TOKUSEI in Japanese 6 Feb 90 pp 33-36

[Article by Hideo Sugiyama, post-graduate course, Nippon University, and Junichi Kaneko and Makoto Sugamata, Production Engineering Section, Nippon University]

[Text] **1. Introduction**

A variety of aluminum-based alloys have reportedly been transformed into the amorphous state by mechanical alloying (MA); however, few attempts have been made to turn, into the amorphous state, particles of intermetallic compounds dispersed in aluminum as the second phase. The present article deals with blending of intermetallic compounds of aluminum and a transition metal with pure aluminum, followed by the MA treatment of the mixture, to allow dispersion of the particles in aluminum, and then with an attempt to transform the dispersed particles in the amorphous state. The intermetallic compounds selected were $FeAl_3$, $NiAl_3$, $TiAl_3$, and $ZrAl_3$, which form equilibrium phases with Al, and TiAl, which does not. The limiting concentrations for these transition metals to form a solid solution with Al are 0.73 at.% for Ti, 0.058 at.% for Zr, 0.025 at.% for Fe, and 0.023 at.% for Ni. Following their MA treatment, these powders were investigated by X-ray diffraction for their constituent phases and by differential scan calorimetry (DSC) analyses for their crystallization temperature; attempts were also made to produce an Al bulk molding with amorphous particles dispersed by means of hot extrusion of the MA powders.

2. Method of Experiment

The composition of the mixtures of powders subjected to the MA treatment are presented in Table 1. The vacuum-arc melting buttons for each of the intermetallic compounds of different compositions were subjected to a homogenization process by heating in vacuum, followed by crushing them mechanically with a mortar and pestle into powders, which were added to atomized aluminum powder of 99.99 percent purity. TiAl exclusively, however, was added as scrapped

pieces. The heating conditions for homogenization were 1,223 K x 562 ks for $FeAl_3$, $TiAl_3$, $ZrAl_3$, and TiAl and 1,073 K x 562 ks for $NiAl_3$.

Table 1. Blending Ratio of Elements for the Specimens

Material	Tr at.%	Addition	At.%	Wt.%
Al–$FeAl_3$	2.5	$FeAl_3$	10	12.7
Al–$NiAl_3$	2.5	$NiAl_3$	10	12.9
Al–$TiAl_3$	2.5	$TiAl_3$	10	11.9
Al–$ZrAl_3$	2.5	$ZrAl_3$	10	15.9
Al–TiAl	3.0	TiAl	6	8.3

The MA treatment was conducted with a high-energy ball mill of the dry type, which was made up of a stainless steel tank of a capacity of 5,000 mℓ containing 18 kg of three-eighth inch-diameter balls made of bearing steel. The tank was equipped with a water-cooled jacket, which prevented to some extent the rise of temperature of the specimens during the MA treatment. One treatment proceeded with 700 gr of powder for the charges, 4.2 gr of stearic acid for the auxiliary agent, Ar gas of gauge pressure 0.3 kg/cm and flow rate of 800 mℓ/minute blown in, and the impeller rotating at 160 rpm continuously for 86.4 ks. The powders under the treatment were picked out in portions at the MA times of 3.6, 10.8, 18.0, 36.0, 54.0, 72.0, and 86.4 ks to examine changes in microstructure, hardness, and constituent phases of the powder being treated.

The microstructure of the MA powder was examined with an optical microscope to learn largely how the intermetallic compound particles were dispersed in the matrix Al. The hardness was tested with a microhardness tester (microVickers, held for 15 seconds at a load of 10 gf) for the surface, polished with a buff, of a specimen that was produced by implanting into a resin an MA powder obtained during the relevant treatment. CuKα beams of 40 kV and 20 mA strength were used for the identification of constituent phases and for the assessment of amorphous transformation. The powder specimens having undergone the 86.5-ks MA treatment had their matrix Al fused with hot phenol; a concentrated material obtained as the residue after filtration of the fused fluid was subjected to DSC thermal analysis and temperatures of crystallization, etc., were determined.

3. Results of Experiments and Discussion

3.1 Microstructure and Hardness of the MA Powder

Since the intermetallic compounds added to the matrix Al are by far harder and more brittle, they were implanted in Al as they were crushed by the MA treatment, and soon gave a uniformly dispersed microstructure. Changes in consistency of the powder in the MA treatment are shown in Figure 1. The hardness continued to rise with increasing time of MA, although it reached near saturation as the MA time approached 86.4 ks. The final hardness differed

somewhat for different intermetallic compounds added, but still remained in the Hv range of 100~140. Figure 2 [not reproduced] presents the structure, as observed by the optical microscope, of powders having undergone the MA treatment for 86.4 ks. In all of the pictures, the second phase particles of the possible intermetallic compound is seen to have dispersed uniformly. Most of them are fine particles of the order of 0.1 μm, although some are comparatively crude and measure several μm. The differences by type of intermetallic compound are not appreciable.

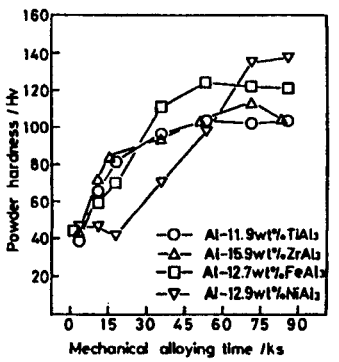

Figure 1. Changes in the Hardness of Powder Resulting From MA Treatment

3.2 Results of the X-Ray Diffraction Test for MA Powders

Results of X-ray diffraction in the range of 2 θ = 20~70° on powders subjected to the MA treatment for 3.6 ks and 54 ks are shown in Figure 3. In case (a), where the intermetallic compound $FeAl_3$ was added, the peaks of the compound were gone after the powder had undergone the 3.6 ks MA treatment; in the case of $NiAl_3$ addition (b), the peaks of the compound were still definitely notable after the 3.6 ks MA treatment, but not after that of 54 ks. In case (c), where $TiAl_3$ was added, the peaks were notable even after 54 ks MA treatment, although the peak intensity was much diminished. Where $ZrAl_3$ was added, the peaks noted after a 3.6 ks MA treatment were gone after a 54 ks treatment. In any case, the diffraction peak intensity representing an intermetallic compound was diminished with extended MA treatment.

Allowing for the two-element phase diagram of the transition metals, it was not conceivable that a new intermetallic compound had developed in the above experiments. It may be concluded either that the intermetallic compound was gone by forming a solid solution of the transition metal and aluminum or that the intermetallic compound had changed to the amorphous state while maintaining the dispersed state of the compound. Changes in lattice parameters were investigated from the diffraction lines of aluminum present in the range 2 θ = 20~70°. The parameters showed that the changes in value after MA treatment were limited, and thus the amount of the compound turned into solid solution was limited in comparison with the one added. It was concluded that, allowing for the microstructures of the MA powders shown in Figure 2 [not reproduced], diffusion of the compound into the Al matrix might scarcely have taken place in the MA treatment and that reduction in tensity of the diffraction lines of the intermetallic compound or their total disappearance after the MA treatment shown in the figure, might have resulted largely

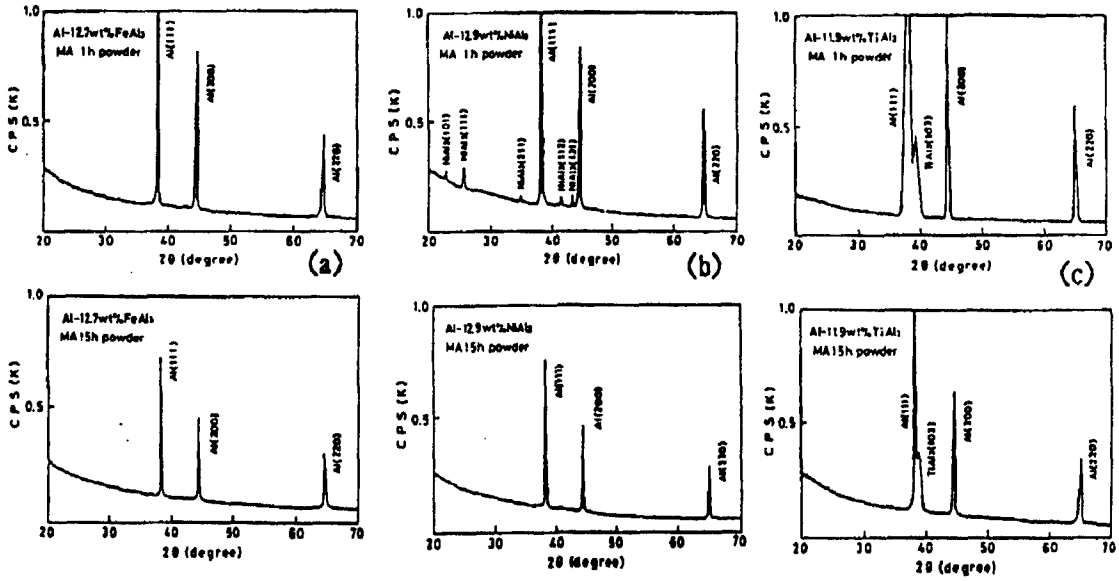

Figure 3. X-Ray Diffraction Patterns of Powders Subjected to MA Treatment (a) $FeAl_3$, (b) $NiAl_3$, (c) $TiAl_3$

from the progress of formation of amorphous material from the phase of intermetallic compound.

3.3 Result of DSC Analysis

The temperatures for crystallization were examined into the amorphous state by the MA treatment. With the volume ratio of the dispersed particles low, at about 10 percent, the Al matrix was dissolved in hot phenol and a concentrated residue obtained therefrom by filtration was used as the specimen, which was first heated at a rate of 10 K per minute up to and beyond the melting point of Al, 933 K, to determine relevant DSC curves. The specimen was then cooled gradually and subjected again to heating under the same conditions, to give a second DSC curve and to compare the first with the second. Resulting DSC curves, as obtained with use of Shimazu-DSC-50 apparatus, are presented in Figure 4. In the case of $FeAl_3$ (a), a small exothermic peak was present at about 560 K, followed by a large one in the vicinity of 710 K, with the latter conceivably representing the exothermic one due to crystallization. At a temperature further up, around 933 K, an endothermic peak accompanying the melting of residual Al was notable. The second DSC curve produced by reheating of the material is shown as the dotted line, which extends flatly up to the Al-melting point, with the exothermic peaks gone. In the case of $NiAl_3$ (b), two peaks were present: one at around 560 K and exothermic; the other at around 710 K and endothermic. The cause for the latter is not yet known, whereas the former may conceivably represent the temperature of crystallization. An exothermic peak was notable at a high temperature, of around 800 K, in the case of $TiAl_3$ (c), and an exothermic peak at around 660 K, as well as an endothermic peak at around 720 K in the case of $ZrAl_3$ (d). The exothermic peak at around 860 K for $TiAl_3$ seems to be too high to be a crystallization temperature, whereas crystallization probably took place at 660 K in $ZrAl_3$.

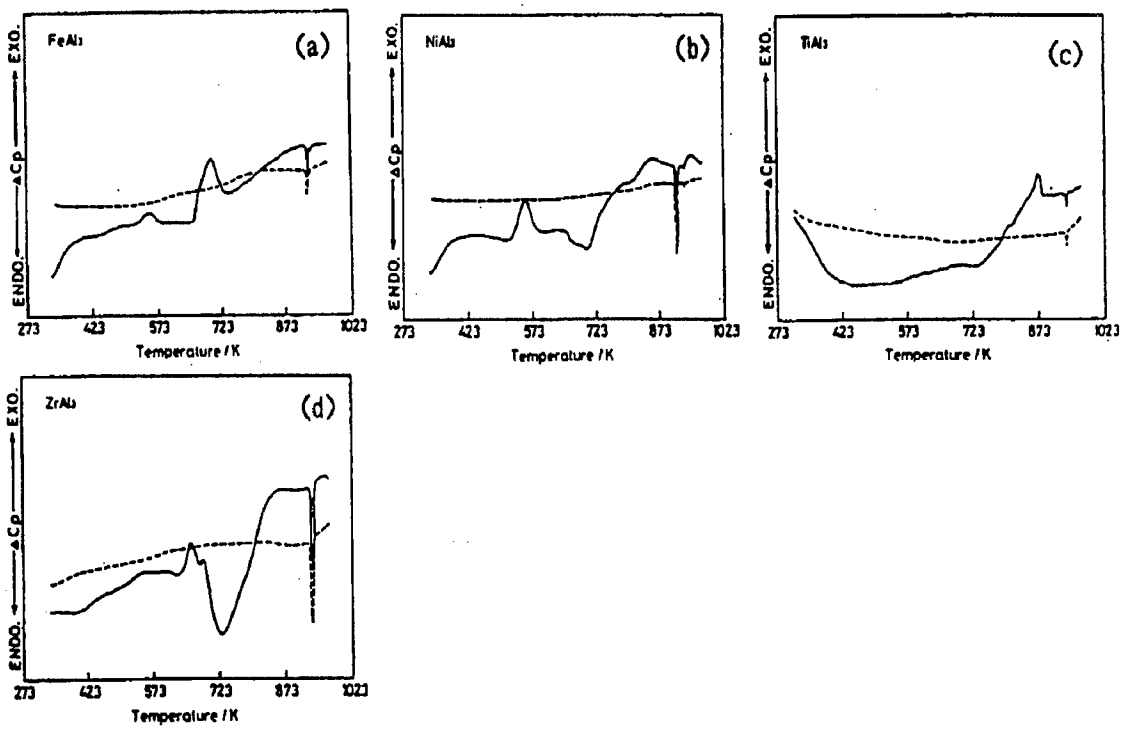

Figure 4. DSC Curves of Powders Subjected to MA Treatment

3.4 Bulk-Material Moldings by Hot Extrusion

Each of the MA powders was subjected to hot extrusion to give a compact bulk molding. The extrusion was performed at a temperature of 573 K, the temperature concluded as the lowest possible one for relevant molding, and at an extrusion ratio of 12, which turned out round rods of 10 mmϕ. Results of X-ray diffraction tests on these extruded rods are shown in Figure 5. Definite diffraction lines representing the intermetallic compounds were notable in all specimens, indicating that the compounds had been crystallized again in the process of the hot extrusion. The temperature for extrusion was lower than that for crystallization estimated from the DSC curves; nevertheless, heating for comparatively long hours combined with the deformation stress applied in extrusion may have led to crystallization.

3.5 Addition of TiAl as the Intermetallic Compound

The powder having undergone MA treatment after addition of the intermetallic compound TiAl, which is incapable of coexisting with Al in an equilibrium state, along with the extruded material of the resultant powder, were tested by X-ray diffraction (results are as shown in Figure 6). No diffraction lines indicating the presence of TiAl were noted in the pattern for the MA powder, which suggested that the added compound was in the amorphous state. The bulk moldings produced by hot extrusion, in turn, showed definite diffraction lines derived from the equilibrium phase $TiAl_3$ as well as from the added TiAl, which suggested that the application of heat allowed formation of $TiAl_3$ at the interface of Al and TiAl.

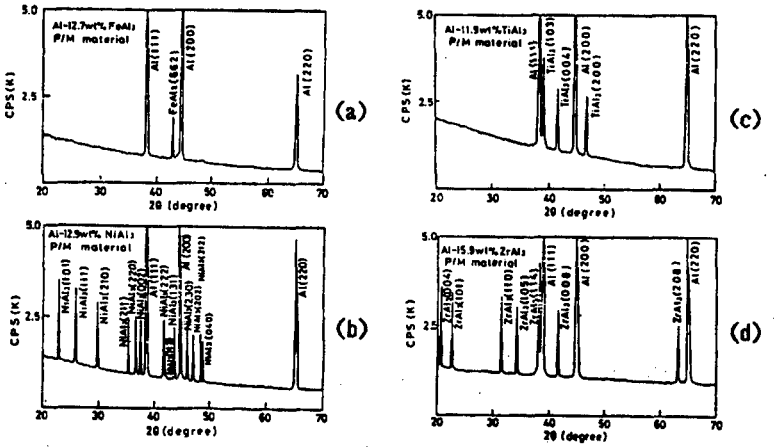

Figure 5. X-Ray Diffraction Patterns for the Powders Subjected to Hot Extrusion

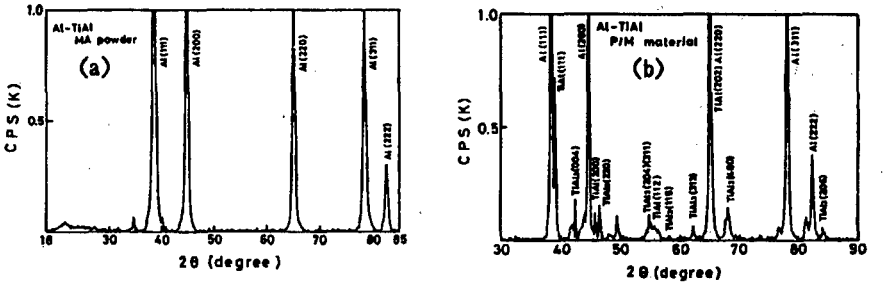

Figure 6. X-Ray Diffraction Patterns for Specimens Involving TiAl
(a) MA powder; (b) Bulk made by hot extrusion

4. Conclusion

It was concluded that MA treatments of a mixture of Al powder and an intermetallic compound allowed the particles of the intermetallic compound finely dispersed in the Al matrix to proceed with its conversion to the amorphous state. An attempt to create an Al bulk molding with dispersed amorphous particles, however, failed because crystallization of the dispersed amorphous particles took place in the course of extrusion and deformation.

Preparation of Al-Cr Amorphous Alloys by Mechanical Alloying Method

906C7531J Tokyo AL KEI AMORUFASU GOKIN NO KOZO TO TOKUSEI in Japanese 6 Feb 90 pp 37-40

[Article by Kojiro Kobayashi, Production and Processing Engineering Section, Technology Department, Nagoya University]

[Text] Amorphous alloys have, in the past, been produced exclusively by either the rapid quench solidification method or by the vapor phase quench method. New methods have, however, emerged for the formation of amorphous powder for some alloy series[1]; one is mechanical alloying (MA) for a mixture of pure elements, and the other is mechanical grinding (MG) where the solidified phase prepared from these elements is crushed with a ball mill, etc. The Al-Cr alloy series is representative of the metal-transition metal series of alloys, the Al-Cr alloy subjected to rapid solidification formed quasicrystallizations in the composition range for chromium of 15~16 at.%,[2] but did not form amorphous material.[2] Nor has the formation of an amorphous material by the solid-phase reaction method been reported to date. By means of the vapor phase quench method exclusively both quasicrystals and amorphous materials have been formed.

The present article deals with the preparation of amorphous materials from Al-Cr series of alloys by MA and MG.

1. Mechanical Alloying of Powders of the Metals Al and Cr

In solid phase reaction MA, the mixture of crystalline elements is converted, by the mechanical energy provided, from a high free-energy state to a lower one of an amorphous state or another semistable state, as seen in Figure 1.

Figure 2 presents X-ray diffraction pictures, varied with the time of MA or ball milling, for an Al-Cr alloy blended into a Cr-composition of 15 at.%. The MA alone allows amorphous material to form in the Al-Ni and Al-Ti series, whereas 1,000 hours of MA still leaves crystalline phases in the Al-Cr series.

Figure 3 presents results of differential scan calorimetry (DSC) for specimens subjected to MA treatment for different periods of time. A gradually rising exothermal peak is notable in the vicinity of 670 K after 800 and 1,000 hours of MA.

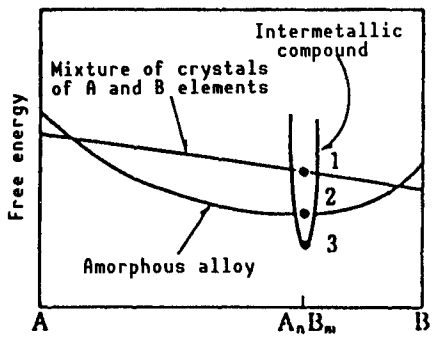

Figure 1. Change of Free Energy in Formation of Amorphous State by MA and MG, as Suggested by Schwarz, et al.[3] (A semistable state, or state 3 in the figure, was experimentally transformed into the amorphous state by providing a mechanical energy.)

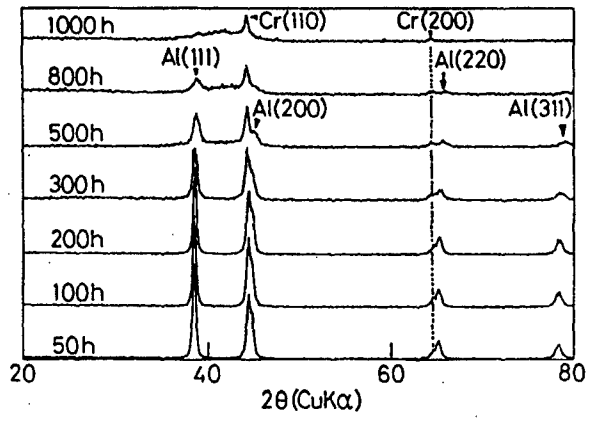

Figure 2. X-Ray Diffraction Picture for the Alloy Al-15at.% Cr Subjected to MA Treatment for Different Hours (Starting from the element powders.)

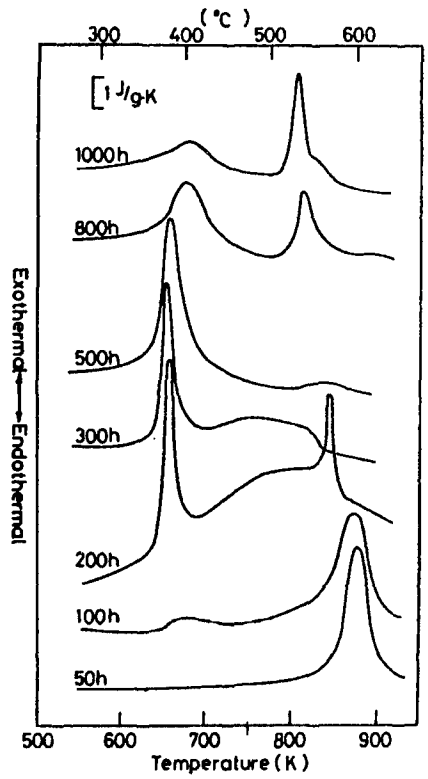

Figure 3. DSC Curves for the Alloy Al-15 at.% Cr Subjected to MA Treatment for Different Hours (Rate of heating: 0.33 K/s)

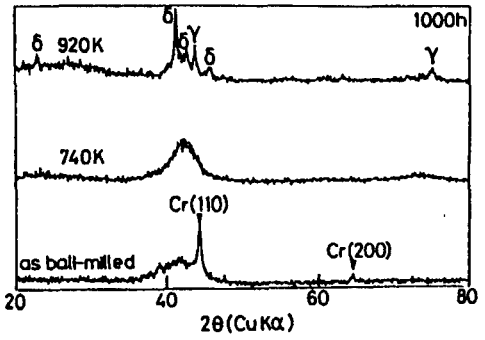

Figure 4. X-Ray Diffraction Picture of the Specimen Subjected to Continuous Heating Up to the Exothermic Peak Temperature of the DSC Curves and Then Quenched to Room Temperature

Figure 4 presents changes seen in X-ray diffraction of the specimen heated just above the DSC peak after it had been subjected to MA treatment for 1,000 hours. The exothermic reaction for the specimen started at around 620 K, as it did for the ones subjected to MA for 200~500 hours, but the shape of the peak was much flatter in the DSC. After heating up to 740 K, just the temperature of the peak on the lower side (in the DSC figure), the peak of the crystallization phase in the diffraction picture vanished, leaving a broad peak of the amorphous phase alone. This amorphous-phase peak was transformed into crystalline phase in the diffraction picture after displaying the second sharp peak in the DSC figure, as the temperature was further raised. The result was identical for MA of 800 hours.

Transmission electron microscopic (SEM) observation of specimens hardened by first heating to 740 K and then by quenching to room temperature showed a single amorphous phase for both the halo ring of the electron diffraction picture and the bright field dark/field picture. The amorphous phase turns into crystal at 800 K with an emitted heat of 2.2 kJ/mol.

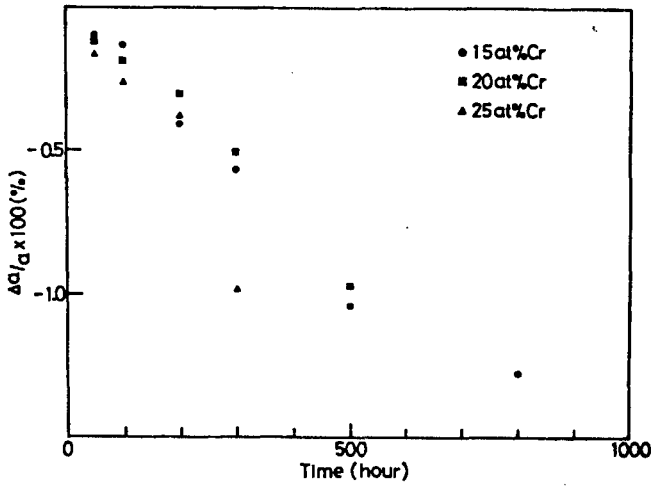

Figure 5. Plot of MA Treatment Time Vs. a Lattice Parameter for Al-Rich Phases of Alloy

The amorphous phase formed by the thermal treatment after the MA treatment above required an activation energy of 190 kJ for the crystallization.

With increasing MA-treatment time, the Al peak in the X-ray diffraction picture shifts to the higher angle side, thereby the Cr peak merging with that of Al to form a solid solution. Figure 5 presents changes of lattice parameters for Al with extending time of MA treatment. The abscissa represents time, and the ordinate the ratio of changes of relevant lattice parameters to those for pure Al. The lattice parameters fall with increasing treatment time, indicating that the formation of solid solution with Cr does not require an activation energy.

2. Mechanical Grinding of the Al-Cr Alloy Subjected to Rapid Quench Solidification

(1) Al-15at.%Cr

Ribbons produced by subjecting the relevant elements to single-roll rapid consolidation at a rate of 10^4~10^5 K/s were crushed and used as the material. The material is made up exclusively of a quasicrystal, which is a semistable phase, and β phase, which is an equilibrium phase.[5]

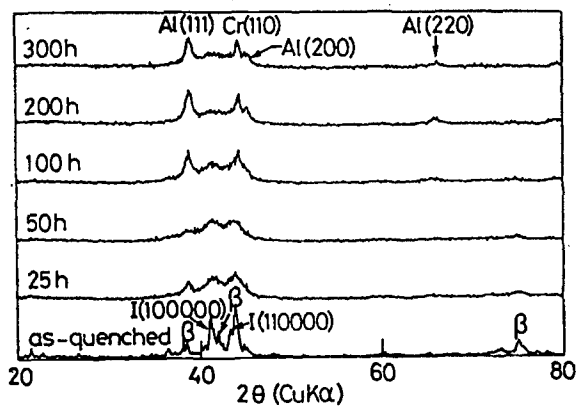

Figure 6. X-Ray Diffraction Picture for the Alloy Al-15at.%Cr Subjected to MA Treatment for Different Hours (Starting from a powder made by crushing of melt spun or quenched ribbons.)

Figure 6 presents X-ray diffraction pictures of relevant Al-15at.%Cr alloy subjected to MG treatment for different hours. With extending MG treatment hours, the crystal peaks gradually crumbled down, peaks for Al and Cr crystals emerged after over 100 hours of MG, and a broad pattern indicating the presence of an amorphous material showed up between Al(111) and Cr(110) after 200 hours or more of MG.

Figure 7 represents DSC curves of the alloy subjected to continuous heating at a rate of 0.33 K/s after it had undergone MG treatment for different hours. The exothermic peak shifted to the high temperature side with extended MG-treatment hours.

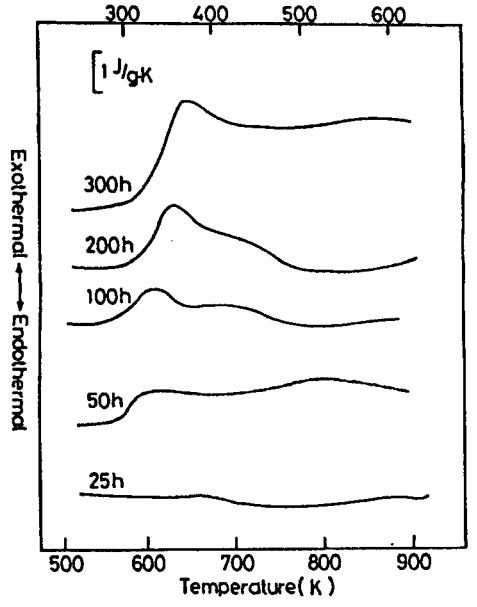

Figure 7. DSC Curves for the Alloy Al–15at.%Cr Subjected to MA Treatment for Different Hours

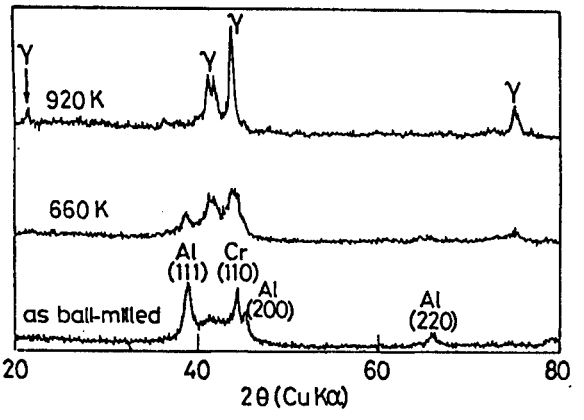

Figure 8. X-Ray Diffraction Picture of the Specimen Subjected to MG Treatment for 300 Hours, Then to a Continuous Heating Up to the Exothermic Peak Temperature of the DSC Curve, and Then to Quenching to Room Temperature

To elucidate the mechanism involved in the exothermic peak, the specimen temperature was raised to just above that of the peak and then rapidly lowered to the level of room temperature, and subsequently subjected to X-ray diffraction measurements.

Figure 8 represents the diffraction picture of a specimen heated continually after a 300-hour MG treatment. A continuous heating up to 660 K showed the appearance of an equilibrated γ phase in place of the amorphous phase. From the specimen temperature of 700 K and above, no distinct peaks were notable; at 920 K, however, the Al peak that had still remained at 660 K was gone and only the γ phase was left. The γ phase already present at 660 K may conceivably have grown gradually, with the Al and Cr peaks absorbed therein.

According to Peterson, et al.,[4] diffusion of Cr in Al goes on with $D_0 = 5 \times 10^{18} nm^2/s$ and $Q = 4 \times 10^{-19} J$. Assuming that the diffusion distance during continuous heating at 0.33 K/s is $X = 2\sqrt{Dt}$, that $D = D_0 \exp(-Q/KT)$, and that the temperature does not change for infinitely short periods, the value X is given by

$$X = \int_{T1}^{T} \sqrt{D_0 \exp(-Q/KT)/a(T-T_0)}\, dt .$$

The diffusion distance upon heating up to 620 K is computed to be 4 Å, a value that agrees well with experimental ones rising rapidly with rising temperature.

(2) Al-20at.%Cr

The ribbons yielded in rapid solidification by the single roll method were made up of a quasicrystal and an equilibrium phase, the γ phase.

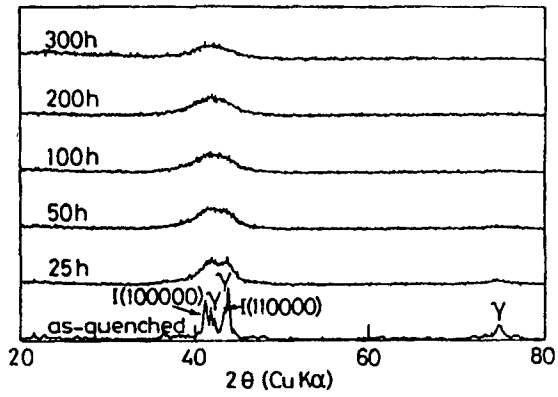

Figure 9. X-Ray Diffraction Picture of the Alloy Al-20at.%Cr Subjected to MG Treatment for Different Hours
(Starting from a powder made by crushing of melt spun ribbons.)

Figure 9 represents X-ray diffraction pictures of Al-20at.%Cr alloy subjected to MG treatment for different hours; it can be seen that the crystal peaks had crumbled down after 24 hours of MG treatment, and were completely gone after 50 hours, with a broad peak of the amorphous phase alone remaining in the range of 2 θ of 37~45°.

Figure 10 represents DSC curves for the alloy having undergone a continuous heating after having been subjected to MG treatment for different hours. An exothermic peak was found in the vicinity of 870 K, which grew sharper and shifted to the higher temperature side as MG treatment time was extended.

Figure 11 resents X-ray diffraction pictures of the alloy having undergone continuous heating after it had undergone MG treatment for 300 hours. After having heated the alloy to 820 K, the temperature just below that of the peak, the amorphous phase was still maintained although the half-value width of the peak was narrowed. With continued heating, the specimen underwent an exothermic reaction involving a crystallization from the amorphous phase into the δ phase, an equilibrium phase.

The heat emitted in crystallization from the amorphous phase to the δ phase, which corresponds to the area of the peak, was 3.2 kJ/mol and the activation energy for the crystallization was 240 kJ/mol.

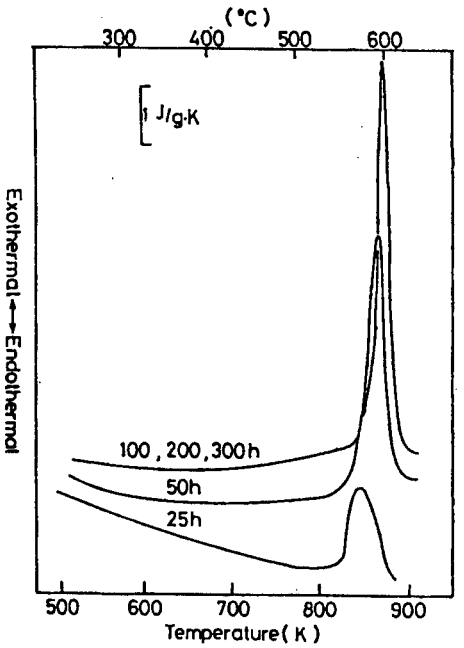

Figure 10. DSC Curves of the Alloy Al–20at.%Cr Subjected to MG Treatment for Different Hours and Then to a Continuous Heating Up to the Exothermic Peak Temperature of the DSC Curves at a Rate of 0.33 K/s

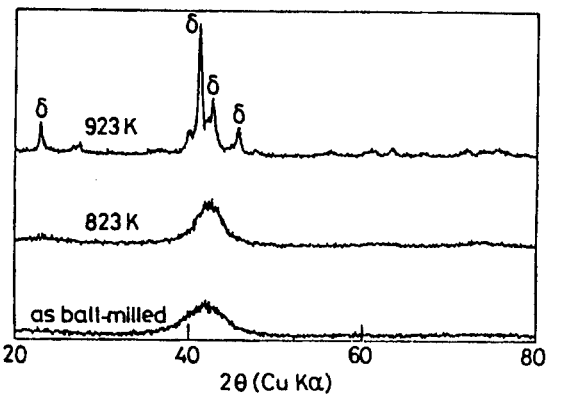

Figure 11. X–Ray Diffraction Picture of Specimens Subjected to MG Treatment for 300 Hours, Then to a Continuous Heating Up to the Exothermic Peak Temperature of the DSC Curve, and Then to Quenching to Room Temperature

References

1. Weeber, A.W. and Bakker, H., PHYSICA B, Vol 153, 1988, p 93.

2. Inoue, A., Kimura, H., and Masumoto., T., J. MATER. SCI., Vol 22, 1987, p 1758.

3. Schwarz, R. and Koch, C.C., APPL. PHYS. LETT., Vol 49, 1986, p 146.

4. Peterson, N.L. and Rothman, S.J., REV., Vol 31, 1970, p 3264.

5. Kobayashi, K.F., Tachibana, N., and Shingu, P.H., J. MATER. SCI., Vol 24, 1989, p 2437.

– END –

Foreign Broadcast Information Service (FBIS) and Joint Publications Research Service (JPRS) publications contain political, military, economic, environmental, and sociological news, commentary, and other information, as well as scientific and technical data and reports. All information has been obtained from foreign radio and television broadcasts, news agency transmissions, newspapers, books, and periodicals. Items generally are processed from the first or best available sources. It should not be inferred that they have been disseminated only in the medium, in the language, or to the area indicated. Items from foreign language sources are translated; those from English-language sources are transcribed. Except for excluding certain diacritics, FBIS renders personal and place-names in accordance with the romanization systems approved for U.S. Government publications by the U.S. Board of Geographic Names.

Headlines, editorial reports, and material enclosed in brackets [ ] are supplied by FBIS/JPRS. Processing indicators such as [Text] or [Excerpts] in the first line of each item indicate how the information was processed from the original. Unfamiliar names rendered phonetically are enclosed in parentheses. Words or names preceded by a question mark and enclosed in parentheses were not clear from the original source but have been supplied as appropriate to the context. Other unattributed parenthetical notes within the body of an item originate with the source. Times within items are as given by the source. Passages in boldface or italics are as published.

SUBSCRIPTION/PROCUREMENT INFORMATION

The FBIS DAILY REPORT contains current news and information and is published Monday through Friday in eight volumes: China, East Europe, Soviet Union, East Asia, Near East & South Asia, Sub-Saharan Africa, Latin America, and West Europe. Supplements to the DAILY REPORTs may also be available periodically and will be distributed to regular DAILY REPORT subscribers. JPRS publications, which include approximately 50 regional, worldwide, and topical reports, generally contain less time-sensitive information and are published periodically.

Current DAILY REPORTs and JPRS publications are listed in *Government Reports Announcements* issued semimonthly by the National Technical Information Service (NTIS), 5285 Port Royal Road, Springfield, Virginia 22161 and the *Monthly Catalog of U.S. Government Publications* issued by the Superintendent of Documents, U.S. Government Printing Office, Washington, D.C. 20402.

The public may subscribe to either hardcover or microfiche versions of the DAILY REPORTs and JPRS publications through NTIS at the above address or by calling (703) 487-4630. Subscription rates will be provided by NTIS upon request. Subscriptions are available outside the United States from NTIS or appointed foreign dealers. New subscribers should expect a 30-day delay in receipt of the first issue.

U.S. Government offices may obtain subscriptions to the DAILY REPORTs or JPRS publications (hardcover or microfiche) at no charge through their sponsoring organizations. For additional information or assistance, call FBIS, (202) 338-6735,or write to P.O. Box 2604, Washington, D.C. 20013. Department of Defense consumers are required to submit requests through appropriate command validation channels to DIA, RTS-2C, Washington, D.C. 20301. (Telephone: (202) 373-3771, Autovon: 243-3771.)

Back issues or single copies of the DAILY REPORTs and JPRS publications are not available. Both the DAILY REPORTs and the JPRS publications are on file for public reference at the Library of Congress and at many Federal Depository Libraries. Reference copies may also be seen at many public and university libraries throughout the United States.